# Scale sensitivity of the Gill circulation, Part I: equatorial case

**Beatriz Reboredo [1], Gilles Bellon [1]**

[1]Department of Physics, University of Auckland, Auckland, New Zealand.

**Key Points:**

- In the limit of a very localized diabatic heating, the Gill circulation exhibits strong low-level westerly jet and overturning circulation.
- In this limit, the overturning circulation is constrained by the balance between vertical energy transport and diabatic heating.
- Both the overturning circulation and the low-level westerly jet weaken with increasing horizontal extent of the diabatic heating.

Corresponding author: Gilles Bellon, `gilles.bellon@auckland.ac.nz`

## Abstract

We investigate the steady dynamical response of the atmosphere on the equatorial $\beta$-plane to a steady, localized, mid-tropospheric heating source at the equator (Part II investigates the off-equatorial case). Expanding Gill (1980)'s seminal work, we vary the latitudinal and longitudinal scales of the diabatic heating pattern while keeping the total amount of diabatic heating fixed. We focus on characteristics of the response which would be particularly important if the circulation interacted with the hydrologic and energy cycles: the overturning circulation and the low-level wind. In the limit of very small scale in either the longitudinal or latitudinal direction, the intensity of the overturning circulation tends towards the value for which the vertical energy transport balances the diabatic heating, which is also the limit in the non-rotating case (with $\beta = 0$). In the same limit, the low-level westerly jet still extends eastward of the center of diabatic heating, while there is no jet in the non-rotating case. The intensity of the overturning circulation decreases with increasing longitudinal or latitudinal scale of the diabatic heating. The low-level westerly jet decreases in maximum velocity and spatial extent relative to the spatial extent of the diabatic heating with increasing longitudinal or latitudinal scale of the diabatic heating, and the associated low-level eastward mass transport decreases with increasing longitudinal scale. Our results suggest that moisture-convergence feedbacks will favor small-scale convective disturbances while surface-heat-flux feedbacks would favor small-scale disturbances in mean westerlies and large-scale disturbances in mean easterlies.



## Plain Language Summary

Most meteorological phenomena in the tropics result from the interaction between moist thermodynamics and dynamics. Indeed, heating by diabatic processes such as phase change and radiation create temperature and pressure gradients which cause atmospheric circulations. These circulations in turn transport water and humidity and by doing so couple with the diabatic processes. This coupling is complex, poorly understood, and poorly simulated by current climate models, with bearings on our understanding and forecast capability of many tropical meteorological phenomena. This study deepens our understanding of one side of this interaction, furthering our knowledge of the dynamical response to steady diabatic heating at the equator. We focus particularly on the influence of the horizontal extent of this heating. We find that the more spread-out the heating, the slower the overturning circulation and low-level westerly winds in the region of diabatic heating. Our results suggest that the coupling of the circulation with the energy and water cycle would favor small convective cloud systems, especially in westerlies.


## 1 Introduction

Gill (1980, hereafter G80)'s seminal work aimed to provide a very simple model of the Walker circulation that results from the longitudinal distribution of diabatic heating in the tropics, with maxima of convective heating over the three equatorial land masses or achipelagos – Amazonia, Africa and the Maritime Continent (Krueger & Winston, 1974) – as well as monsoon circulations resulting from off-equatorial regional diabatic heating. G80 showed that the damped, linear, baroclinic dynamical response of the tropical atmosphere to a localized, steady, mid-tropospheric diabatic heating reproduces the main features of these circulations.

This simple model has become one of the main frameworks to understand tropical circulations and its solutions are now commonly called Gill circulation. The relevance of G80's work to the atmospheric circulation associated with El Niño Southern Oscillation was revealed soon after the publication of the original article (Pazan & Meyers, 1982; Philander, 1983) and it lead to a leap in our understanding of El Niño Southern

Oscillation (Cane & Zebiak, 1985). Later studies of the dynamical pattern associated with the Madden-Julian Oscillation (MJO) (Madden & Julian, 1971; C. Zhang, 2005) revealed that this pattern is essentially G80's equatorially symmetric solution (Hendon & Salby, 1994; Kiladis et al., 2005). Very recently, this framework has shown promise to understand the observed pattern of tropical precipitation in details (Adam, 2018). Because of this widespread relevance, G80's model has come to be considered foundational, and is used as a test for further theoretical development (e.g., Bretherton & Sobel, 2003).

G80 mostly focused on two cases, with latitudinal distributions of diabatic heating for which there are simple solutions: one symmetric about the equator, the other asymmetric. This constrained the horizontal scale of the heating. Gill (1980) and Heckley and Gill (1984) presented a couple more cases with little analysis. Further generalisations of G80's work attempted to simulate the observed flow realistically (Z. Zhang & Krishnamurti, 1996), with some success. Even if the Gill circulation appears relevant to observed large-scale tropical circulations, these circulations span a significant range of horizontal scales, and we have yet to understand how sensitive the Gill circulation is to the horizontal extent and latitude of the imposed diabatic heating. The present work aims to address this question, with a particular focus on characteristics of the circulation that interact with the energy cycle: the vertical, overturning circulation which is associated with moisture transport and latent heat release, and the surface wind which modulates the surface turbulent heat fluxes.

In the present article, we explore the sensitivity of Gill's equatorially symmetric circulation, leaving off-equatorial cases to Part II Bellon and Reboredo (2020). In Section 2, we present the Matsuno-Gill equation system and its solutions, as well as the non-rotating case. Section 3 presents some solutions as well as the scale sensitivity of the overturning circulation and of the low-level wind. Section 4 summarizes our findings and concludes.

## 2 Method

We use the vertical structure of Quasi-equilibrium Tropical Circulation Models (QTCM) (Neelin & Zeng, 2000; Zeng et al., 2000; Lintner et al., 2012) to derive parameters of the equation system for the steady first baroclinic response of the tropical atmosphere to prescribed diabatic heating, over a $\beta$-plan. We present semi-analytical solutions for a more general case than in G80, i.e., applicable to heating of varied horizontal extents, to shed some light on the nature and amplitude of the dynamical response. In this section, we summarize the equations of the model and the method of solutions by decomposition in cylinder functions. We also solve the non-rotating case as a reference, and study the asymptotes for small zonal extent of the diabatic heating.

### 2.1 Linear baroclinic model of the tropical atmosphere

In the QTCM, the tropospheric temperature is assumed to differ from a reference profile $T_{\mathrm{r}}(p)$ by an anomaly with fixed profile $a_1(p)$ which corresponds to a moist adiabat up to the upper troposphere where a cold-top effect is included: $T(x, y, p, t) = T_{\mathrm{r}}(p) + a_1(p)\, T_1(x, y, t)$. The vertical profile of velocity is assumed to be identical to the profile of geopotential gradients, which is linked to the profile of temperature anomaly by the hydrostatic approximation. Details of the models can be found in (Neelin & Zeng, 2000; Zeng et al., 2000; Lintner et al., 2012).

The equation for the baroclinic velocity $\mathbf{v}_1$ is:

$$\partial_t \mathbf{v}_1 + f\mathbf{k} \times \mathbf{v}_1 = -R\nabla T_1 - \epsilon_1 \mathbf{v}_1, \tag{1}$$

where $f = \beta y$ is the Coriolis parameter, $\mathbf{k}$ the vertical unit vector, $R$ is the gas constant for air, and $\epsilon_1$ is a coefficient for linear damping due to viscosity and the projection of surface friction on the first baroclinic mode.

The temperature equation is:

$$\langle a_1 \rangle \partial_t T_1 + M_{\text{sr}1} \nabla \cdot \mathbf{v}_1 = \langle Q \rangle - \langle a_1 \rangle \epsilon_1 T_1, \tag{2}$$

where $\langle\ \rangle$ indicates the vertical average over the troposphere, $M_{sr1}$ is the base-state gross dry static stability for the baroclinic mode normalized by the heat capacity of air (computed using the reference temperature profile $T_{\text{r}}$), $Q$ is the diabatic heating rate, and $\epsilon_1$ is a damping coefficient accounting for Newtonian cooling. The damping coefficients for temperature and momentum are set to be equal as in G80.

The momentum and temperature Equations (1) and (2) can be non-dimensionalized using the speed of gravity waves $c = (RM_{\text{sr}1}/\langle a_1 \rangle)^{1/2}$ and the equatorial Rossby radius $\mathcal{L} = (c/2\beta)^{1/2}$, so that the resulting non-dimensional set of equations is identical to the linear shallow-water equations used in G80 (with the surface pressure replaced by the mid-tropospheric temperature) for the steady state. The characteristic time scale is $\tau = \mathcal{L}/c = (2\beta c)^{-1/2}$ and the temperature scale is $\mathcal{T} = M_{\text{sr}1}/\langle a_1 \rangle$. With

$$\begin{gathered} x = \mathcal{L}\hat{x}, \qquad y = \mathcal{L}\hat{y}, \qquad t = \tau\hat{t}, \\ \mathbf{v}_1 = c\hat{\mathbf{v}}, \qquad T_1 = \mathcal{T}\hat{T}, \qquad \hat{\epsilon} = \epsilon_1\tau, \qquad \hat{Q} = \tfrac{\tau}{M_{sr1}}\langle Q \rangle, \end{gathered} \tag{3}$$

where $\hat{}$ denotes non-dimensional variables, we have

$$\partial_{\hat{t}}\hat{\mathbf{v}} + \frac{1}{2}\hat{y}\mathbf{k} \times \hat{\mathbf{v}} = -\hat{\nabla} \cdot \hat{T} - \hat{\epsilon}\mathbf{v}, \tag{4}$$

$$\partial_{\hat{t}}\hat{T} + \hat{\nabla} \cdot \hat{\mathbf{v}} = \hat{Q} - \hat{\epsilon}\hat{T}. \tag{5}$$

If we neglect the damping in the meridional momentum equation (its order of magnitude allows for this approximation) and consider the steady state, these equations are equivalent to Equations (2.6), (2.8), and (2.12) in G80:

$$\epsilon u - \frac{1}{2}yv = -\frac{\partial T}{\partial x}, \tag{6}$$

$$\frac{1}{2}yu = -\frac{\partial T}{\partial y}, \tag{7}$$

$$\epsilon T + \frac{\partial u}{\partial x} + \frac{\partial v}{\partial y} = Q, \tag{8}$$

where the $\hat{}$ have been omitted to maximize the similarity with G80's notations. We will keep these notations without $\hat{}$ for the rest of the article. We will take $\epsilon = 0.1$ as in G80. This damping rate was at times assessed to be too large (e.g., Battisti et al., 1999), but more recent studies have shown that such a value is justified, in particular because of convective momentum transport (Lin et al., 2005, 2008). The non-dimensional upward mid-tropospheric vertical velocity is equal to the non-dimensional baroclinic divergence and can be written:

$$w = Q - \epsilon T. \tag{9}$$

### 2.2 Solutions to cylinder-shaped forcing

G80 showed the analytical solutions to Equations (6)-(8) for diabatic heatings that follow half a period of a cosine function in the zonal direction and a parabolic cylinder function in the meridional direction:

$$Q^{(n)} = F(x)D_n(y) \text{ with } n \in \mathbb{N}, \tag{10}$$

and $F$ a half-period of cosine function in a limited range of longitude:

$$F(x) = \begin{cases} k\cos(kx) & \text{for } |x| < L_x, \\ 0 & \text{for } |x| > L_x, \end{cases} \text{ with } k = \frac{\pi}{2L_x}, \tag{11}$$

and $D_n$ a parabolic cylinder function of degree $n$, i.e., the product of a polynomial of degree $n$ and an exponential that limits the latitudinal extent of the significant diabatic heating:

$$\begin{aligned} D_0 &= \exp\left(-\frac{y^2}{4}\right), \\ D_1 &= y\exp\left(-\frac{y^2}{4}\right), \\ D_{n+1} &= yD_n - nD_{n-1}, \quad \forall n > 0 \end{aligned} \tag{12}$$

Note that our function $F$ differs from the function $F$ in G80 by a factor $k$ which we introduced to make the integral of $F$ over the longitude independent from $k$.

The method of solution as described in G80 introduces two new variables $q$ and $r$ that combine $T$ and $u$ in the Equations (6)-(8) as:

$$q = T + u, \tag{13}$$

$$r = T - u. \tag{14}$$

For each forcing following a parabolic cylinder function $Q^{(n)} = F(x)D_n(y)$, the solutions $(q^{(n)}, v^{(n)}, r^{(n)})$ can be written as the sum of two additive components (Gill, 1980; Heckley & Gill, 1984; Abramowitz & Stegun, 1964), $(q^{(n,1)}, v^{(n,1)}, r^{(n,1)})$ in which $q^{(n,1)}$ is proportional to $D_n(y)$, $v^{(n,1)}$ is proportional to $D_{n-1}(y)$, and $r^{(n,1)}$ is proportional to $D_{n-2}(y)$, and $(q^{(n,2)}, v^{(n,2)}, r^{(n,2)})$ in which $q^{(n,2)}$ is proportional to $D_{n+2}(y)$, $v^{(n,2)}$ is proportional to $D_{n+1}(y)$, and $r^{(n,2)}$ is proportional to $D_n(y)$:

$$q^{(n)} = q^{(n,1)} + q^{(n,2)} = q_n^{(n)}(x)D_n(y) + q_{n+2}^{(n)}(x)D_{n+2}(y), \tag{15}$$

$$v^{(n)} = v^{(n,1)} + v^{(n,2)} = v_{n-1}^{(n)}(x)D_{n-1}(y) + v_{n+1}^{(n)}(x)D_{n+1}(y), \tag{16}$$

$$r^{(n)} = r^{(n,1)} + r^{(n,2)} = r_{n-2}^{(n)}(x)D_{n-2}(y) + r_n^{(n)}(x)D_n(y) \tag{17}$$

The longitudinal functions in the first component are solutions of:

$$\frac{dq_n^{(n)}}{dx} - (2n-1)\epsilon q_n^{(n)} = -(n-1)F(x), \tag{18}$$

$$v_{n-1}^{(n)} = 2n\epsilon q_n^{(n)} - nF(x), \tag{19}$$

$$r_{n-2}^{(n)} = nq_n^{(n)}. \tag{20}$$

And in the second component, they are solutions of:

$$\frac{dq_{n+2}^{(n)}}{dx} - (2n+3)\epsilon q_{n+2}^{(n)} = -F(x), \tag{21}$$

$$v_{n+1}^{(n)} = 2(n+2)\epsilon q_{n+2}^{(n)} - F(x), \tag{22}$$

$$r_n^{(n)} = (n+2)q_{n+2}^{(n)}. \tag{23}$$

Equations (19), (20), (22) and (23) give the solutions as a function of $q_n^{(n)}$ and $q_{n+2}^{(n)}$ and the heating's longitudinal distribution $F$, so solving Equations (18) and (21) gives the complete solution $q^{(n)}$ that involves $q_n$, $q_{n+2}$, $v_{n-1}$, $v_{n+1}$, $r_{n-2}$, and $r_n$ for $n > 1$. The same combinations without the functions with negative indices for $n = 0$ and $n = 1$ are the solutions studied in G80, with heating symmetric ($n = 0$) and asymmetric ($n = 1$) with respect to the equator.

For $n = 0$, the longitudinal dependence of the first component can be written:

$$\{\epsilon^2 + k^2\} q_0^{(0)} = \begin{cases} 0 & \text{if } x < -L_x, \\ \epsilon k \cos(kx) + k^2 \sin(kx) + k^2 \exp[-\epsilon(x + L_x)] & \text{if } |x| < L_x, \\ 2k^2 \cosh(\epsilon L_x) \exp\{-\epsilon x\} & \text{if } x > L_x, \end{cases} \tag{24}$$

for $n = 1$:

$$q_1^{(1)} = 0, \tag{25}$$

and for $n > 1$:

$$\frac{(2n-1)^2\epsilon^2 + k^2}{n-1} q_n^{(n)} = \begin{cases} 2k^2 \cosh[(2n-1)\epsilon L_x] \exp[(2n-1)\epsilon x] & \text{if } x < -L_x, \\ (2n-1)\epsilon k \cos(kx) - k^2 \sin(kx) + k^2 \exp[(2n-1)\epsilon(x - L_x)] & \text{if } |x| < L_x, \\ 0 & \text{if } x > L_x. \end{cases} \tag{26}$$

Note that only $q_0^{(0)}$ is non-zero east of the region of diabatic heating, and zero west of it. All other components extend west of the region of heating.

It is clear from the similarity of Equations (18) and (21) and from the same boundary and continuity conditions that apply to $q_n^{(n)}$ and $q_{n+2}^{(n)}$ that the longitudinal dependence of the second component can be written, for all $n$:

$$q_{n+2}^{(n)} = \frac{1}{n+1} q_{n+2}^{(n+2)}, \tag{27}$$

i.e. the longitudinal dependence of the second component of the response to heating along $D_n$ is proportional to the longitudinal dependence of the first component of the response to heating along $D_{n+2}$

To get back to the physical non-dimensional variables, we use $T^{(n)} = (q^{(n)} + r^{(n)})/2$ and $u^{(n)} = (q^{(n)} - r^{(n)})/2$. The first component of the solution is, for $n = 0$:

$$\left.\begin{aligned} u^{(0,1)} &= T^{(0,1)} = \frac{1}{2} q_0^{(0)}(x) D_0(y), \\ v^{(0,1)} &= 0; \end{aligned}\right\} \tag{28}$$

for $n = 1$:

$$\left.\begin{aligned} u^{(1,1)} &= T_1^{(1,1)} = 0, \\ v^{(1,1)} &= -F(x) D_0(y); \end{aligned}\right\} \tag{29}$$

for $n > 1$, it is

$$\left.\begin{aligned} T^{(n,1)} &= \frac{1}{2}q_n^{(n)}(x)[D_n(y) + nD_{n-2}(y)], \\ u^{(n,1)} &= \frac{1}{2}q_n^{(n)}(x)[D_n(y) - nD_{n-2}(y)], \\ v^{(n,1)} &= n[2\epsilon q_n^{(n)}(x) - F(x)]D_{n-1}(y); \end{aligned}\right\} \tag{30}$$

And the solution for the second component is, for all $n$:

$$\left.\begin{aligned} T^{(n,2)} &= \frac{1}{2}q_{n+2}^{(n)}(x)[D_{n+2}(y) + (n+2)D_n(y)], \\ u^{(n,2)} &= \frac{1}{2}q_{n+2}^{(n)}(x)[D_{n+2}(y) - (n+2)D_n(y)], \\ v^{(n,2)} &= [2(n+2)\epsilon q_{n+2}^{(n)}(x) - F(x)]D_{n+1}(y). \end{aligned}\right\} \tag{31}$$

Following from Equation (27), it is straightforward that the second component of the temperature and zonal wind response to heating along $D_n$ has the same patterns as the first component of the response to heating along $D_{n+2}$: $T^{(n,2)} = T^{(n+2,1)}/(n+1)$ and $u^{(n,2)} = u^{(n+2,1)}/(n+1)$.

Both components' contributions to the mid-tropospheric vertical velocity can be written:

$$w^{(n,m)} = \frac{1}{2}F(x)D_n(y) - \epsilon T^{(n,m)}, \tag{32}$$

for all $n$ and for $m = 1$ or 2.

Note that:

1. Only the first component of the solution for $n = 0$ extends beyond $x = L_x$ in the longitudinal direction. It is associated with no meridional wind and has a Kelvin-wave structure as noted in G80.
2. All other components have a Rossby-wave structure with gyres aligned in the longitudinal band of the diabatic heating and west of it, with a westward extent that decreases with $n$. On each side of the equator, cyclonic and anticyclonic gyres alternate in the poleward direction.
3. For $n$ even, the gyres straddling the equator rotate in the same meteorological direction, cyclonic or anticyclonic, for both components. The total number of gyres is $n$ for the first component and $n$+2 for the second component. If the gyres closest to the equator in the first component are cyclonic, the gyres closest to the equator in the second component are anticyclonic and vice-versa. This is due to the change of signs of $D_{2n}(0)$ with every increment in $n$ (see Eq. (A5)).
4. For $n$ odd, the gyres on each side of the equator have opposite directions of rotation (one is cyclonic, the other anticyclonic) for both components. The total number of gyres is $n$+1 for the first component and $n$+3 for the second component. If the gyres just north of the equator in the first component are cyclonic, the gyres just south of the equator in the second component are cyclonic (same if anticyclonic). This is due to the change of signs of $D_{2n+1}$ near $y = 0$ with every increment in $n$ (see Eqs. (A4)-(A5)).

### 2.3 More general forcing

Because of the variety of scales of cloud ensembles, it is of interest to understand the dynamical response to diabatic heating with a wide range of horizontal extent from the synoptic to the planetary scale. The present work expands on the results of G80 for diabatic heating symmetric about the equator by studying the response to diabatic heating $Q$ with a similar shape as the symmetric case ($n = 0$) in G80 (half-period cosine in the longitudinal direction, Gaussian in the meridional direction), but with varying longitudinal and meridional extents:

$$Q = F(x)D(y), \tag{33}$$

with $F(x)$ in the form given by Equation (11), and $D(y)$ a Gaussian function in the form:

$$D(y) = \frac{1}{L_y} \exp\left(-\frac{y^2}{4L_y^2}\right). \tag{34}$$

With such a formulation, the imposed heating $Q$ is a "patch" of heating centered on the equator (Part II treats the case of an off-equatorial heating). The heating pattern is close to circular for $L_x = 3L_y$. By design, the maximum heating varies with $L_x$ and $L_y$ in $k/L_y$ but the total heating imposed to the atmosphere is independent of the longitudinal and latitudinal scales: the energy input in the global atmosphere is the same in all cases:

$$[Q] = \int_{-L_x}^{+L_x} \int_{-\infty}^{+\infty} Q dxdy = 4\sqrt{\pi}, \tag{35}$$

with the brackets $[\cdot]$ indicating global integration.

With inner product $\langle f, g \rangle = \int f g \, dy$, $D_n$ functions form an orthogonal basis $(D_n)_{n\in\mathbb{N}}$. The norm of each $D_n$ is $\sqrt{n!\sqrt{2\pi}}$. The Gaussian function $D$ can be decomposed in a series on the basis $(D_n)_{n\in\mathbb{N}}$:

$$\begin{aligned} D(y) &= \sum_{n=0}^{\infty} a_n(L_y) D_n(y), \\ \text{with } a_{2n} &= \frac{1}{2^n n!} \left(\frac{L_y^2 - 1}{L_y^2 + 1}\right)^n \sqrt{\frac{2}{L_y^2 + 1}}, \\ \text{and } a_{2n+1} &= 0 \text{ for } n \in \mathbb{N}. \end{aligned} \tag{36}$$

It is straightforward that $Q$ can also be written as a series of $Q^{(n)}_{n\in\mathbb{N}}$:

$$Q = \sum_{n=0}^{\infty} a_n Q^{(n)} F(x), \tag{37}$$

with $a_n = 0$ for $n$ odd in our case with diabatic heating symmetric about the equator (see Eq. (34)).

The solution to the steady, linear equation system (6)-(8) forced by $Q = F(x)D(y)$ can be determined semi-analytically as an infinite sum of the solutions to the diabatic heatings $Q^{(n)} = F(x)D_n(y)$:

$$T = \sum_{n=0}^{\infty} a_n T^{(n)}, \tag{38}$$

$$u = \sum_{n=0}^{\infty} a_n u^{(n)}, \tag{39}$$

$$v = \sum_{n=0}^{\infty} a_n v^{(n)}. \tag{40}$$

In practice, and since the infinite sum in Equation (36) is convergent, it can be approximated by a finite sum up to a value $m$ following a convergence criterion (Cauchy, 1821). The convergence criterion requires to set a positive error of tolerance $\delta$ for which any index $l \geqslant m+1$ satisfies $|| \sum_{n=0}^{l} a_n(L_y)D_n(y) - \sum_{n=0}^{l-1} a_n(L_y)D_n(y)|| \leqslant \delta$ at $y = 0$. This value $m$ will differ for different values of $L_y$. For example, setting $\delta = 0.001$, one mode is enough for the trivial case where $L_y = 1$, whereas for $L_y = 0.5$ we need 10 modes to meet the error criterion, and more modes are needed for smaller $L_y$. (Heckley & Gill, 1984) used the same approach to study the transient response to a very localized heating.

### 2.4 A baseline: the non-rotating case

One of the crucial elements of the Gill circulation is the longitudinal asymmetry which results from the rotation of the Earth. It is therefore interesting to be able to evaluate the exact effects of rotation. To do so, we also solve the non-rotating case. If we neglect the Coriolis acceleration, the system reduces to a classical damped gravity wave. Equations (4) and (5) easily reduce to:

$$\begin{aligned} w &= -\frac{1}{\epsilon}\Delta T, && (41)\\ T &= \frac{1}{\epsilon}Q + \frac{1}{\epsilon^2}\Delta T. && (42) \end{aligned}$$

These equations make clear that, in the absence of any circulation, the temperature response is reduced to the direct thermodynamic response $Q/\epsilon$. Vertical energy transport adds a diffusive term $\Delta T/\epsilon^2$ to the temperature response; as a result, the large-scale transport damps temperature gradients and the equilibrium temperature response to a diabatic heating is spatially smoother than the diabatic heating itself.

The damped gravity wave response to a forcing described by Equation (33) can be obtained by decomposing the latitudinal dependence of $Q$ through a Fourier transform. We get:

$$D(y) = \frac{1}{\sqrt{\pi}} \int_{-\infty}^{+\infty} e^{-\ell^2 {L_y}^2} \cos(\ell y)\, d\ell, \tag{43}$$

and we can then write the equilibrium temperature response as a Fourier decomposition in $y$ as well:

$$T = \frac{1}{\sqrt{\pi}} \int_{-\infty}^{+\infty} \mathcal{T}_\ell(x)\, e^{-\ell^2 {L_y}^2} \cos(\ell y)\, d\ell, \tag{44}$$

and each function $\mathcal{T}_\ell$ is solution to:

$$\lambda^2 \mathcal{T}_\ell - \partial_{xx}\mathcal{T}_\ell = \epsilon\, F(x), \tag{45}$$

with $\lambda^2 = \left(\epsilon^2 + \ell^2\right)$. This second-order linear differential equations can be solved for $x < -L_x$, $|x| < L_x$, and $x > L_x$. The solutions to the corresponding homogeneous equation are $e^{\pm\lambda x}$, and a particular solution proportional to $\cos(kx)$ for $|x| < L_x$ is easily found. By using continuity conditions at $x = \pm L_x$ and evanescent conditions for $x \longrightarrow \pm\infty$, the general solution can be derived:

$$\left(\lambda^2 + k^2\right)\ \mathcal{T}_\ell\ = \begin{cases} \epsilon k \cos(kx) + \epsilon \frac{k^2}{\lambda}\, e^{-\lambda L_x} \cosh(\lambda x) & \text{if } |x| < L_x, \\ \epsilon \frac{k^2}{\lambda} \cosh(\lambda L_x)\, e^{-\lambda |x|} & \text{if } |x| > L_x. \end{cases} \tag{46}$$

The corresponding winds can be written in a Fourier decomposition as well:

$$\begin{aligned} u &= \frac{1}{\sqrt{\pi}} \int_{-\infty}^{+\infty} \mathcal{U}_\ell(x)\, e^{-\ell^2 {L_y}^2} \cos(\ell y)\, d\ell, \\ v &= \frac{1}{\sqrt{\pi}} \int_{-\infty}^{+\infty} \mathcal{V}_\ell(x)\, e^{-\ell^2 {L_y}^2} \sin(\ell y)\, d\ell, \\ w &= \frac{1}{\sqrt{\pi}} \int_{-\infty}^{+\infty} \mathcal{W}_\ell(x)\, e^{-\ell^2 {L_y}^2} \cos(\ell y)\, d\ell, \end{aligned} \tag{47}$$

with

$$\left(\lambda^2 + k^2\right) \mathcal{U}_\ell = \begin{cases} k^2 \sin(kx) - k^2\, e^{-\lambda L_x} \sinh(\lambda x) & \text{if } |x| < L_x, \\ \mathrm{sgn}(x) k^2 \cosh(\lambda L_x)\, e^{-\lambda |x|} & \text{if } |x| > L_x, \end{cases} \tag{48}$$

$$\mathcal{V}_\ell = \frac{\ell}{\epsilon} \mathcal{T}_\ell, \tag{49}$$

and

$$\left(\lambda^2 + k^2\right) \mathcal{W}_\ell = \begin{cases} \left(\ell^2 + k^2\right) k \cos(kx) - \epsilon^2 \frac{k^2}{\lambda}\, e^{-\lambda L_x} \cosh(\lambda x) & \text{if } |x| < L_x, \\ -\epsilon^2 \frac{k^2}{\lambda} \cosh(\lambda L_x)\, e^{-\lambda |x|} & \text{if } |x| > L_x. \end{cases} \tag{50}$$

We can point to some similarities between the solutions $q_n$ to Gill circulation and the solutions $\mathcal{T}_\ell$ to the non-rotating problem: they are the sum of a cosine function and an exponential within the heating region, and an exponential decay out of this region, if non zero. In the non-rotating case, the cosine component clearly appears as the primary, local response to the forcing (it is a particular solution of the equation) that does not systematically respect temperature continuity and mass continuity at the zonal boundaries of the region of diabatic heating. The exponential component is the secondary response that ensures mass balance and thermal continuity. In the Gill circulation, an additional terms in sine appears as a result of the symmetry-breaking $\beta$ effect. The characteristic scale for the exponential decay ($(2n-1)\epsilon$ or $(2n+3)\epsilon$ in the rotating case, $\lambda$ in the non-rotating case) combines the damping rate $\epsilon$ and information on the meridional structure of the mode ($n$ in the rotating case, $\ell$ in the non-rotating case): the decay is faster for larger meridional variability (i.e., larger $n$ or larger wavenumber $\ell$). This factor also appears in the amplitude of the response, which is inversely proportional to the sum of the square of this factor and $k^2$. There are also significant differences: in the non-rotating case, the solution is symmetric in the longitudinal direction, unlike in the rotating case. The damped gravity wave's horizontal wind is also irrotational, while the Gill circulation has obvious rotational structures.

### 2.5 Limits for small zonal extent of the heating

Here, we explore the asymptotic solutions for $L_x \rightarrow 0$, focusing on the interval $-L_x \leq x \leq L_x$. Outside this interval, there is no simple expression for the infinite sums or integrals of exponentially decreasing modes which are solutions. Qualitatively, there is subsidence outside of $[-L_x, L_x]$ in both the rotating and non-rotating cases.

**Damped gravity wave:**

For $L_x \to 0$, $k \to +\infty$, and

$$\begin{aligned} \mathcal{T}_\ell \sim \frac{\epsilon}{\lambda}, \qquad & \mathcal{V}_\ell \sim \frac{\ell}{\lambda}, \\ \mathcal{U}_\ell & \sim \sin kx, \\ \mathcal{W}_\ell & \sim k\cos kx, \end{aligned} \tag{51}$$

for $|x| \leq L_x$. It follows through the inverse Fourier transforms that:

$$u \sim \sin(kx)\, D(y), \tag{52}$$

$$w \sim k\cos(kx)\, D(y) = Q, \tag{53}$$

i.e., at first order the temperature perturbation is negligible in front of the diabatic heating and advective cooling. The ascending region is well approximated by the diabatic heating region. Note that Equations (52) and (53 are valid for any function $D$.

**Gill circulation:**

For $L_x \to 0$ and $k \to +\infty$, we have:

$$\begin{aligned} q_0^{(0)} & \sim 1 + \sin kx, \\ q_n^{(n)} & \sim (n-1)(1-\sin kx) \text{ for } n > 0, \\ q_{n+2}^{(n)} & \sim (1-\sin kx) \text{ for all } n, \end{aligned} \tag{54}$$

for $|x| \leq L_x$. Noting that:

$$\begin{aligned} D_n + nD_{n-2} &= -\frac{1}{n-1}\left(D_n - n\, y\, D_{n-1}\right) \text{ for } n > 1 \text{ and} \\ D_{n+2} + (n+2)D_n &= D_n + y\, D_{n+1}, \end{aligned}$$

we can write the temperature responses to cylindrical forcing as follows:

$$\begin{aligned} T^{(0,1)} & \sim \frac{1}{2}(1+\sin kx)\, D_0(y), \\ T^{(1,1)} & \sim 0 \\ T^{(n,1)} & \sim -\frac{1}{2}(1-\sin kx)\left[D_n(y) - n\, y\, D_{n-1}(y)\right] \text{ for } n > 1, \\ T^{(n,2)} & \sim \frac{1}{2}(1-\sin kx)\left[D_n(y) + y\, D_{n+1}(y)\right]. \end{aligned} \tag{55}$$

By combining the odd cylinder function following Equation (12), we can further write:

$$T^{(0)} \sim \frac{1}{2}(1-\sin kx)\; y^2\, D_0(y) + D_0(y), \tag{56}$$

$$T^{(n)} \sim \frac{1}{2}(1-\sin kx)\; y^2\, D_n(y) \text{ for } n > 0. \tag{57}$$

By multiplying $T^{(n)}$ by $a_n$ and summing over $n$, we get the asymptote of the solution $T$ for $L_x \to 0$:

$$T \sim \frac{1}{2}(1-\sin kx)\; y^2\, D(y) + a_0 D_0(y). \tag{58}$$

This result is valid for all functions $D$, not only the symmetric Gaussian used in the rest of this article, with $a_0$ understood as the projection coefficient of $D$ onto $D_0$. A scale analysis reveals the first order for $w$: $\epsilon T = \mathcal{O}(D)$, while $Q = \mathcal{O}(D/L_x)$ so that $\epsilon T << Q$, as in the non-rotating case, and:

$$w \sim k\cos(kx)\, D(y) = Q. \tag{59}$$

The asymptotes for the zonal and meridional wind can be obtained using Equations (6) and (7):

$$u \sim -2\,(1-\sin kx)\left[D(y)+\frac{y}{2}\frac{dD}{dy}\right]+a_0D_0(y), \qquad (60)$$

$$v \sim -k\cos(kx)\,y\,D(y), \qquad (61)$$

valid for any function $D$. For a heating following a symmetric Gaussian (Eq. (34)), of interest in the present work, Equation (60) further simplifies into:

$$u \sim -2\,(1-\sin kx)\left(1-\frac{y^2}{4L_y^2}\right)D(y)+a_0D_0(y), \qquad (62)$$

which is negative around the equator, indicating upper-tropospheric easterlies and low-level westerlies in this region. The zonal wind is maximum on the equator on the western boundary of the heating region ($x=-L_x$), and it decreases both eastward and poleward, eventually changing sign.

If $L_y \to 0$ as well, all the results above hold, and the first term on the right-hand side of the last equation is dominant negligible: the velocity scales with $1/L_y$ and the jets extends in longitude all the way to the eastern boundary of the heating region ($x = L_x$) and in latitude to $y = 2L_y$ on both sides of the equator. This clearly shows that the Gill response is different from a damped gravity wave, even for scales that are much smaller than the equatorial radius of deformation: it is characterized by a westerly low-level jet at the center of the diabatic heating. This suggests significant limitations on the approach considering that small systems in the equatorial regions are well approximated by non-rotating systems.

### 2.6 Additional experiments

We also used both a linear and a non-linear versions of the QTCM on a $\beta$-plane (Sobel & Neelin, 2006; Bellon & Sobel, 2008, 2010; Bellon, 2011) reduced to its baroclinic structure to verify our results by integrating the simplified QTCM in time from an initial state of rest until it reaches a steady state, which is achieved after about 15 days of simulation. With the linear, simplified QTCM, we obtained very similar results to our analytical derivations, which gives us high confidence in our results. In particular, we performed simulations with small zonal and/or meridional extents $L_x$ and $L_y$, and their similarity with the semi-analytical solutions confirms the validity of the longwave approximation down to very small scales. We also performed the same simulations with the non-linear simplified QTCM and found that the results were very similar to the linear version for amplitudes of the forcing up to the typical seasonal heating rates in the observed tropical atmosphere. This shows that the influence of non-linearities is very limited in this problem for realistic amplitudes of the forcing. All these additional experiments demonstrate the robustness of our analytical approach, and we will not show these results in details since they only validate G80's simplifications and confirm our semi-analytical results presented in the next section.

## 3 Results

### 3.1 Temperature and wind response

We present here the features of the solutions in terms of temperature, surface winds and mid-tropospheric vertical motion for diabatic heating distributions $Q$ with different horizontal extents. Figure 1 depicts contours of temperature perturbation and surface velocity field for the damped gravity wave forced by heating of different meridional scales, but with the same total, horizontally integrated heating $[Q]$: $L_y = 1$ (equato-

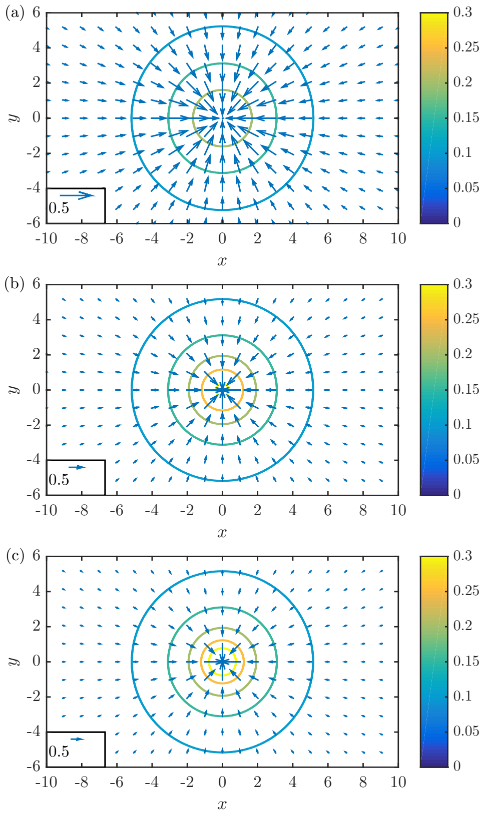


Figure 1: Solutions for the damped gravity wave (non-rotating case): (non-dimensional) temperature response (contours) and low-level velocity (vectors) for (a) $L_y = 1$, (b) $L_y = 1/2$, and (c) $L_y = 1/4$. In all cases, $L_x = 3L_y$.

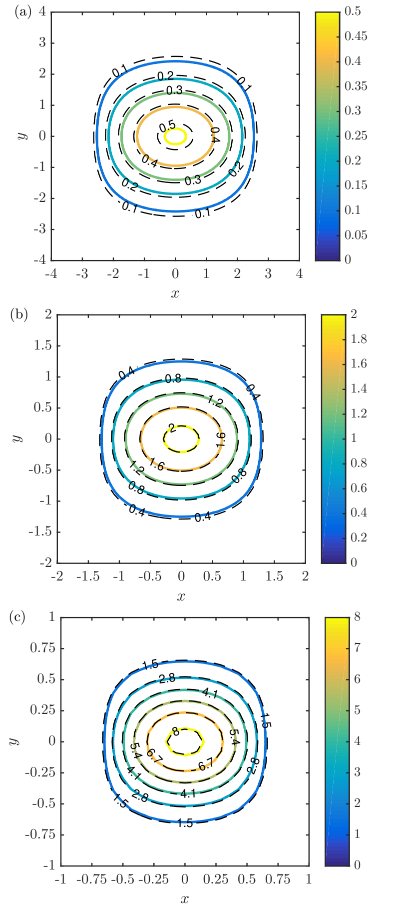


Figure 2: Forcing and solution for the damped gravity wave (non-rotating case): diabatic heating (dashed lines) and mid-tropospheric vertical velocity (solid lines) for (a) $L_y = 1$ (equatorial radius of deformation), (b) $L_y = 1/2$, and (c) $L_y = 1/4$. In all cases, $L_x = 3L_y$.

rial radius of deformation, Fig. 1a), $L_y = 1/2$ (Fig. 1b), and $L_y = 1/4$ (Fig. 1c), with a fixed aspect ratio so that $L_x = 3L_y$ (diabatic-heating pattern close to circular). Figure 2 shows the corresponding contours of mid-tropospheric vertical velocity together with contours of heating. Figures 3 and 4 show the same fields for the Gill circulation (i.e., with rotation). Figures 3a and 4a are almost identical to the symmetric forcing presented in G80, the only difference being the longitudinal extent: $L_x = 3$ here while G80 showed solutions for $L_x = 2$.

The damped gravity wave exhibits a near-circular, warm temperature perturbation collocated with the heating, which forces convergent surface winds (Fig. 1) and ascent collocated with the heating (Fig. 2). The Gill circulation exhibits the Kelvin-wave easterlies east of the heating and cyclonic gyres straddling the equator west of the heating, with maxima of temperature at the center of the gyres, as described in G80 (Fig. 3).

As expected, the temperature and wind fields are symmetric in latitude and longitude for the damped gravity wave (Figs. 1 and 2), while the longitudinal symmetry

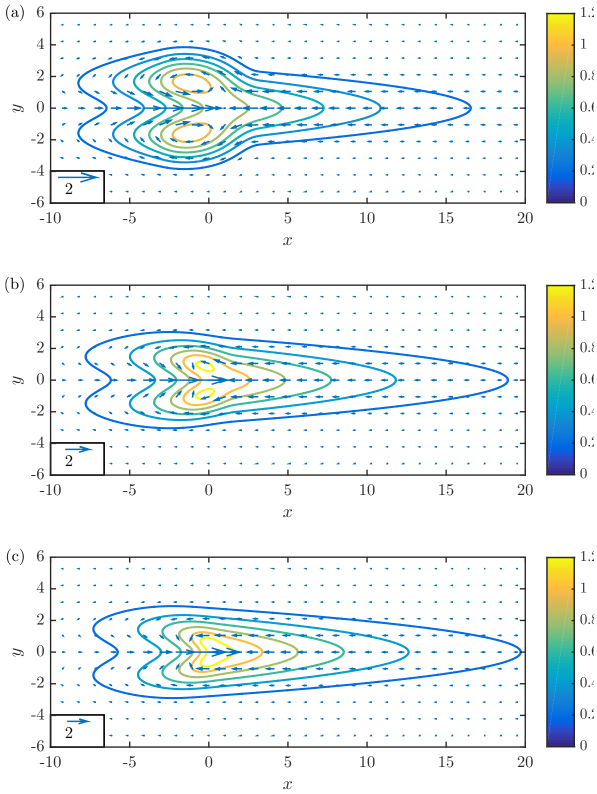

Figure 3: Solutions for the Gill circulation (rotating case): (non-dimensional) temperature response (contours) and low-level velocity (vectors) for (a) $L_y = 1$ (equatorial radius of deformation), (b) $L_y = 1/2$, and (c) $L_y = 1/4$. In all cases, $L_x = 3L_y$.

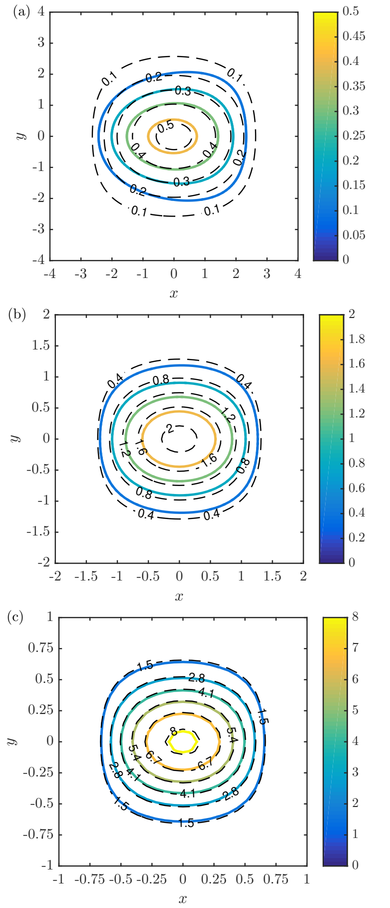

Figure 4: Forcing and solution for the Gill circulation (rotating case): diabatic heating (dashed lines) and mid-tropospheric vertical velocity (solid lines) for (a) $L_y = 1$, (b) $L_y = 1/2$, and (c) $L_y = 1/4$. In all cases, $L_x = 3L_y$.

is broken in the Gill circulation (Figs. 3 and 4). As a result, vertical ascent is more collocated with the heating in the damped gravity wave than in the Gill circulation and therefore more efficient at reducing the temperature response, and the horizontal winds forced by smaller temperature gradients are weaker in the non-rotating case than in the rotating case. The meridional extent of the damped-gravity-wave winds is larger than that of the Gill circulation, and conversely the longitudinal extent of the Gill circulation is larger than that of the damped gravity wave.

As the horizontal extent of the diabatic heating is decreased, the maximum heating scales with $L_x^{-1}L_y^{-1}$. In the damped gravity wave, winds get stronger but more localized (Fig. 1). The maximum vertical speed increases slightly faster than the maximum heating (Fig. 2), and the maximum temperature response increases only slightly (Fig. 1) because of the competition between diabatic warming and advective cooling. In the Gill circulation, winds also get stronger as the horizontal extent of the heating is decreased, especially the equatorial westerly jet between the gyres (Fig. 3), and the maximum vertical speed increases faster than the maximum heating (Fig. 4). The off-equatorial temperature maxima are moved closer to the equator and slightly eastward, they even merge for small $L_y$ (Fig. 3). Overall, the meridional extent of the response decreases. The eastward extent of the temperature and horizontal-wind response increases and the westward extent decreases slightly with decreasing horizontal extent of the heating (Fig. 3). This reveals a decrease in the Rossby-wave response in the west, while the Kelvin-wave response expands eastward. The latter corresponds to an increase in the projection of $D$ on $D_0$ with decreasing $L_y$, which is consistent with the expression of $a_0$ (see Eq. (36)).

Some aspects of the Gill circulation more closely resemble the damped gravity wave for small horizontal extents of the heating: the pattern and amplitude of vertical speed are similar (Figs. 4c and 2c), and the merging of temperature maxima at the equator (Fig. 3c). This could be expected since it extends over a smaller range of latitude around the equator, which corresponds to a region of smaller Coriolis parameter where the effect of rotation should be smaller. But some differences between the Gill circulation and the damped gravity wave are also enhanced: the westerly jet at the center of the heating, the ratio of meridional to zonal extent, and the east-west asymmetry.

### 3.2 Overturning Circulation

One of the most important characteristics of a tropical circulation is its overturning circulation, because of the associated latent heat transport and the coupling with the hydrologic cycle. We define the intensity of the overturning circulation $\Gamma$ as the upward vertical mass flux integrated over the horizontal domain (which, by mass conservation, is the same as the downward vertical mass flux integrated over the domain):

$$\Gamma = \iint_{w>0} w \, dx \, dy. \tag{63}$$

$\Gamma$ can be computed numerically using the expression of $w$ in Equations (32) and (50).

Figure 5a shows the intensity $\Gamma$ of the overturning circulation for the non-rotating case, as a function of the characteristic longitudinal and latitudinal extents $L_x$ and $L_y$ of the heating. For the damped gravity wave, $\Gamma$ decreases with both $L_x$ and $L_y$, in a similar fashion for both. This can be qualitatively understood from Equations (41) and (42): the direct, local temperature response $Q/\epsilon$ is smoother if the features of $Q$ are smoother, i.e. for large horizontal extents $L_x$ and/or $L_y$. The diffusive, smoothing effect of transport $\Delta T/\epsilon^2$ on $T$ is smaller if the features of $T$ are smoother, so that the difference $w = Q - \epsilon T$ is smaller for smoother $Q$. This smaller vertical speed translates into a weaker overturning circulation $\Gamma$ through spatial integration.

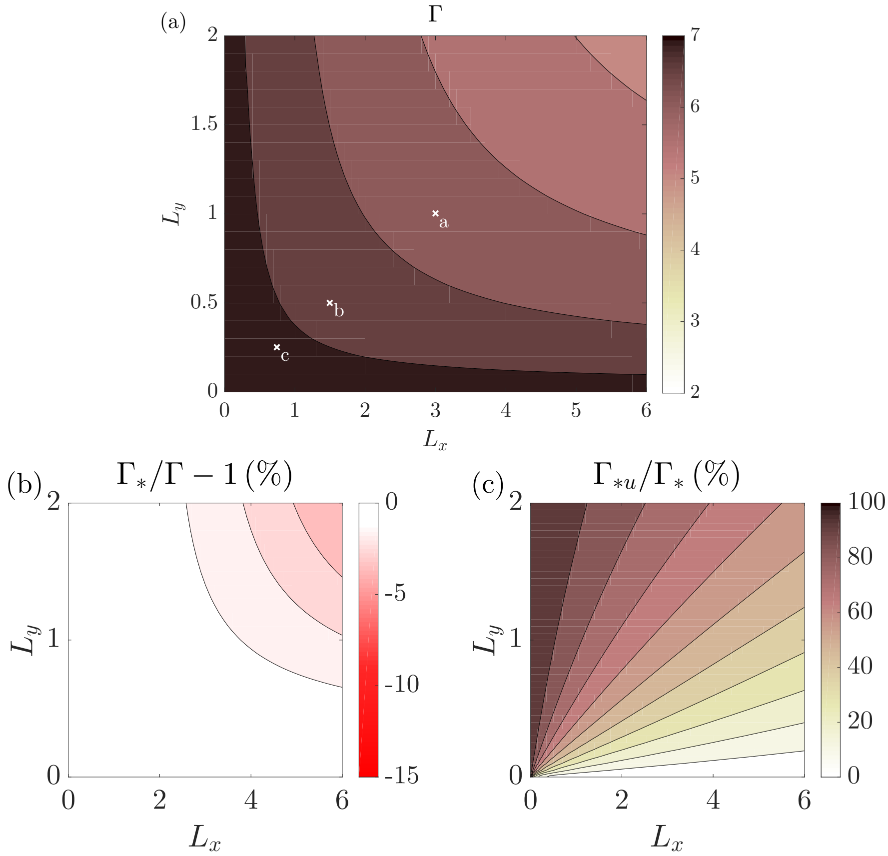


Figure 5: (a) Intensity $\Gamma$ of the overturning circulation in the non-rotating case; the letters "a", "b", and "c" indicate the cases shown in Figures 1 and 2. Contours interval 0.5; (b) Error made by approximating $\Gamma$ by $\Gamma_*$; and (c) Contribution $\Gamma_{*u}$ of the zonal flow to the overturning circulation (in % of $\Gamma_*$).

A more quantitative understanding can be hindered by the fact that the domain of integration in Equation (63) is determined by the field $w$ itself, which we know only as a Fourier decomposition. But Figure 2 suggests that the upward motion is limited to a region between $-L_x$ and $L_x$ in longitude, with a meridional extent that scales with $L_y$. We find that $\Gamma$ can be approximated by the integral $\Gamma_*$ of $w$ over the domain ( $[-L_x,L_x]$,$[-4L_y,4L_y]$ ), with the latitudinal bounds corresponding to twice the e-folding distance of $D$:

$$\Gamma \approx \Gamma_* = \int_{-4L_y}^{4L_y} \int_{-L_x}^{L_x} w \, dx \, dy. \tag{64}$$

Figure 5b shows the normalized error that arises from approximating $\Gamma$ by $\Gamma_*$. This error is negligible for most of the domain of ($L_x$,$L_y$) considered here, topping at 4% for the largest values of $L_x$ and $L_y$, and $\Gamma_*$ can safely be used as an approximation of $\Gamma$. Such a set domain of integration for $\Gamma_*$ presents two noteworthy advantages. First, we can study the contribution of the different spectral modes to $\Gamma_*$:

$$\Gamma_* = 4 \int_{-\infty}^{+\infty} \Gamma_*^\ell(L_x)\, S^\ell(L_y)\, d\ell, \tag{65}$$

with:

$$\Gamma_*^\ell = \int_0^{+L_x} \mathcal{W}^\ell \, dx \quad \text{and} \quad S^\ell = \frac{e^{-\ell^2 L_y{}^2}}{\sqrt{\pi}} \int_0^{+4L_y} \cos(\ell y)\, dy = \frac{e^{-\ell^2 L_y{}^2}}{\sqrt{\pi}} \frac{\sin(4\ell L_y)}{\ell};$$

Note that $S^\ell$ is the integral between 0 and $4L_y$ of the spectral contribution of wavenumber $\ell$ to the diabatic heating (cf Eq. (43)). This means that $\Gamma_*^\ell$ encapsulates the sensitivity of the dynamical response of wavenumber $\ell$. Also, we have the following mathematical constraint on $S^\ell$ for all $L_y$:

$$\int_{-\infty}^{+\infty} S^\ell d\ell = \int_0^{+4L_y} D(y)\, dy \; = 2 \int_0^{+2} e^{-s^2} \, ds = \sqrt{\pi}\, \mathrm{erf}(2), \tag{66}$$

in which we have used the change of variable $s = y/2L_y$.

Second, thanks to the continuity equation, the double integral in Equation (64) is equal to the sum of the integral of $u$ on the longitudinal boundaries and the integral of $v$ on the meridional boundaries of the integration domain and we can look at the contributions of zonal winds and meridional winds to $\Gamma_*$ and $\Gamma_*^\ell$:

$$\Gamma_* = \Gamma_{*u} + \Gamma_{*v} \quad \text{and} \quad \Gamma_*^\ell = \Gamma_{*u}^\ell + \Gamma_{*v}^\ell$$

Integrating Equations (48) and (49), we can write the contributions $\Gamma_{*u}^\ell$ from the zonal winds and $\Gamma_{*v}^\ell$ from the meridional winds to the overturning circulation of the spectral mode $\ell$ as:

$$\Gamma_{*u}^\ell = \frac{k^2}{\lambda^2 + k^2} \frac{1 + e^{-2\lambda L_x}}{2}, \tag{67}$$

$$\Gamma_{*v}^\ell = \frac{\ell^2}{\lambda^2 + k^2} \left( 1 + \frac{k^2}{\lambda^2} \frac{1 - e^{-2\lambda L_x}}{2} \right), \tag{68}$$

which yields the following expression for $\Gamma_*^\ell$:

$$\Gamma_*^\ell = \frac{1}{\lambda^2 + k^2} \left( k^2 + \ell^2 - \frac{\epsilon^2 k^2}{\lambda^2} \frac{1 - e^{-2\lambda L_x}}{2} \right), \tag{69}$$

Figure 5c shows the ratio $\Gamma_{*u}/\Gamma_*$ which illustrates the contribution of the zonal winds to the intensity of the overturning circulation. As expected considering the horizontal isotropy of the non-rotating case, the contribution of the zonal wind to the overturning circulation $\Gamma_*$ is about half for heating patterns which are close to circular (and the contribution of meridional winds is about half as well in these cases) and increase with increasing $L_y$ and decreasing $L_x$.

Section 2.5 shows that for $L_x \to 0$, the temperature response is negligible compared to the diabatic heating, and $w \sim Q$. In this limit, the ascending region becomes the region of heating, and there is no flow through the meridional boundaries (also, $w \sim \partial_x u$), the overturning circulation results at first order from the divergence of the zonal wind:

$$\Gamma \sim [Q] \sim \Gamma_u \text{ and } \Gamma_v \sim 0 \tag{70}$$

This also means that $\Gamma(0, L_y)$ is independent of $L_y$, which is visible in Figure 5a. Equations (67)-(69) confirm that the approximation $\Gamma \approx \Gamma_*$ holds well in this limit: for $L_x \to 0$, $k \to \infty$, $\Gamma_*^\ell = \Gamma_{*u}^\ell = 1$ and $\Gamma_{*v}^\ell = 0$. We can rewrite $\Gamma_*$ using Equation (65) as proportional to the integral of $S^\ell$ over $\ell$, which is given by Equation (66): $\Gamma_*(0, L_y) = \Gamma_{*u}(0, L_y) = 4\sqrt{\pi}\, \mathrm{erf}(2) = \mathrm{erf}(2)[Q] \approx 0.995[Q]$. Our solutions for $\Gamma$ also converge numerically towards $[Q]$ for $L_y \to 0$, which is expected since the non-rotating mathematical system is isotropic and functions $F$ and $D$ both tend towards a Dirac $\delta$ function when the horizontal scale ($L_x$ or $L_y$) tends towards zero.

For $L_x \to \infty$, $k \to 0$ and $\Gamma_*^\ell \to \frac{\ell^2}{\lambda^2}$ which is zero for $\ell = 0$ and tends towards 1 for $\ell \to \infty$. Figure 6a shows the variation of $\Gamma_*^\ell$ with the meridional wavenumber $\ell$ and the zonal extent $L_x$ of the diabatic heating; $\Gamma_*^\ell$ is very close to 1 for $\ell > 0.3$ (i.e. meridional wavelengths shorter than 20, which is approximately the pole-to-pole distance). This corresponds to similar sensitivities of $\Gamma_*^\ell$ to the zonal wavenumber $k = \pi/2L_x$ and to the meridional wavenumber $\ell$, which consistent with our interpretation of the isotropic, diffusive effect of circulation on temperature. There is still some differences between the sensitivities to $k$ and to $\ell$ due to the finite band of longitudes $[-L_x, L_x]$ receiving diabatic heating compared to its latitudinal distribution extending to infinity. Only the small wavenumbers/large wavelengths have a response that is decreasing significantly with $L_x$, with a maximum decrease for $\ell = 0$. The decrease in $\Gamma_*$ with increasing $L_x$ therefore results from the amount of diabatic heating that forces a response projecting onto small wavenumbers $\ell$. Figure 6b shows the variation of the the spectral coefficient $S^\ell$ with the meridional wavenumber $\ell$ and the meridional extent $L_y$ of the diabatic heating. For $\ell L_y << 1$, $S^\ell$ varies almost linearly with $L_y$: $S^\ell \approx 4L_y$; $S^\ell$ also changes sign for $\ell L_y = n\pi/4$ for $n > 0$ (contours of $S^\ell = 0$ can be seen in Fig. 6b for $n = 1$ and 2). As $L_y$ increases, $D$ becomes less peaked at $y = 0$ and the amplitudes of the dynamical response from modes with small wavenumbers $\ell$ increase as a result of the diffusive effect of vertical energy transport in latitude, while the amplitudes of the responses from modes with large wavenumbers $\ell$ decrease. This increases the sensitivity of the circulation intensity $\Gamma$ to $L_x$ and since $\Gamma_*(0, L_y)$ is independent of $L_y$, $\Gamma_*$ decreases with $L_y$.

Figure 7a shows the intensity $\Gamma$ of the overturning circulation in rotating case, as a function of the characteristic extents of the heating $L_x$ and $L_y$: $\Gamma$ decreases with both increasing $L_x$ and $L_y$, in a similar trend for both. For $L_x \to 0$ or $L_y \to 0$, $\Gamma$ is very similar to the non-rotating value. As shown in Section 2.5, in the limit $L_x \to 0$, $\Gamma \sim [Q]$ in both cases. It appears that $\Gamma = [Q]$ is verified in the limit $L_y \to 0$ as well; it is tempting to attribute this limit to the fact that the circulation is confined at the equator where the effect of rotation might be negligible. But Section 2.5 also shows that this argument does not apply in the limit of diabatic heating of very small horizontal extent (with $L_x$ and $L_y \to 0$). In this limit, the Gill circulation differs from the damped gravity wave by a strong low-level westerly jet in the region of heating and the similarity between the damped gravity wave and the Gill circulation in this limit is restricted to the region and intensity of ascent. This argument probably does not apply for cases with $L_x > 0$ and a justification to $\Gamma \sim [Q]$ for $L_y \to 0$ still eludes us.

$\Gamma$'s decrease with increasing $L_x$ and $L_y$ is much steeper in the rotating case than in the non-rotating case. Figure 7b shows the ratio between $\Gamma$ in the rotating case and $\Gamma$ in the non-rotating case; it decreases significantly for increasing $L_x$ and $L_y$, from 1 for $L_x = 0$ or $L_y = 0$ and down to 0.4 for the largest values in the range of parameters we have explored ($(L_x, L_y) = (6, 2)$). Rotation increases the sensitivity of the overturning circulation to the horizontal extent of the diabatic heating pattern. In fact, Figure 3 shows that rotation creates gyres straddling the equator, which are mostly rotational, while the damped gravity wave is exclusively divergent. The poleward flow associated with these gyres seems to compensate most of the equatorward flow and we expect the meridional wind to contribute little to the divergence of the horizontal wind and upward motion. We can also propose an energetic interpretation of this sensitivity. The energy source of the system is the diabatic heating, and the sinks are the kinetic energy loss through friction and the thermal energy loss through Newtonian cooling, the sum of which is proportional to the total energy (kinetic and thermal). Assuming the global thermal energy (and thermal energy loss) is similar in the non-rotating and rotating cases, the global kinetic energy is similar in both cases. In the non-rotating vase, all kinetic energy cor-

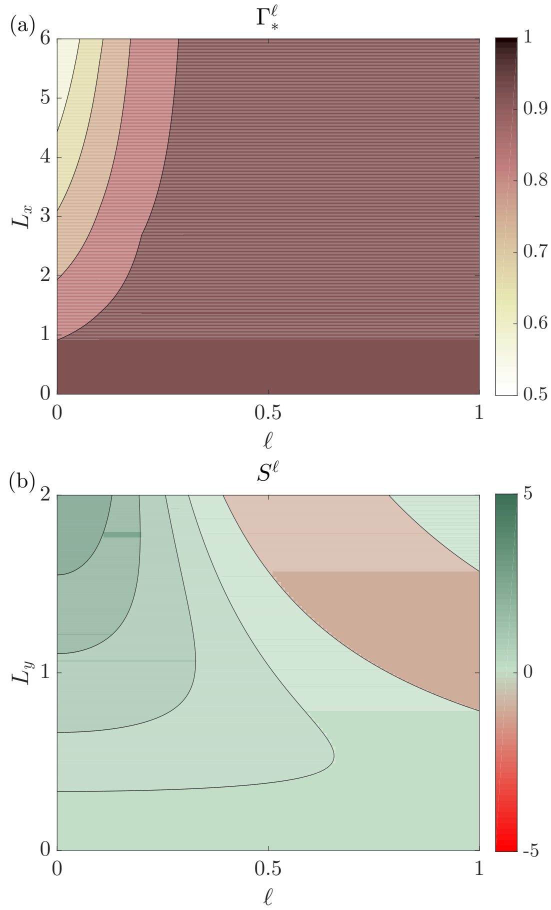


Figure 6: (a) Overturning circulation $\Gamma_*^\ell$ of mode with meridional wavenumber $\ell$ as a function of $\ell$ and the zonal extent $L_x$ of the diabatic heating and (b) spectral coefficient $S^\ell$ as a function of $\ell$ and the meridional extent $L_y$ of the diabatic heating.

responds to divergent motion while in the rotating case part of it is associated with rotational motion and the kinetic energy of divergent motion is smaller than in the rotating case. We can therefore expect the divergent flow to be weaker in the rotating case than in the non-rotating case. There are two caveats to this energy reasoning: first, our semi-analytical solutions to the linear equations do not satisfy energy conservation; second, the kinetic energy loss due to meridional winds is neglected by the longwave approximation. The additional numerical experiments described in Section 2.6 show that these caveats are inconsequential: non-linear, energy-conserving simulations are very similar to our quasi-analytical solutions, which shows that these approximately satisfy energy conservation, and confirms that effect of friction on meridional winds is indeed negligible.

Again, we find that $\Gamma$ can be approximated by the integral $\Gamma_*$ of $w$ over the domain ( $[-L_x,L_x]$,$[-4L_y,4L_y]$ ), although there is more discrepancy between the two than in the non-rotating case. Figure 7c shows the error made by approximating $\Gamma$ by $\Gamma_*$. It is up to 16%, for very large characteristic scales in both meridional and zonal direction, in a range of parameters that correspond to heating that both extend to the extratropics and over a significant fraction of the Earth's circumference (more than a quarter) and is too large to be realistic. $\Gamma_*$ is therefore still a reasonable approximation to $\Gamma$. As in

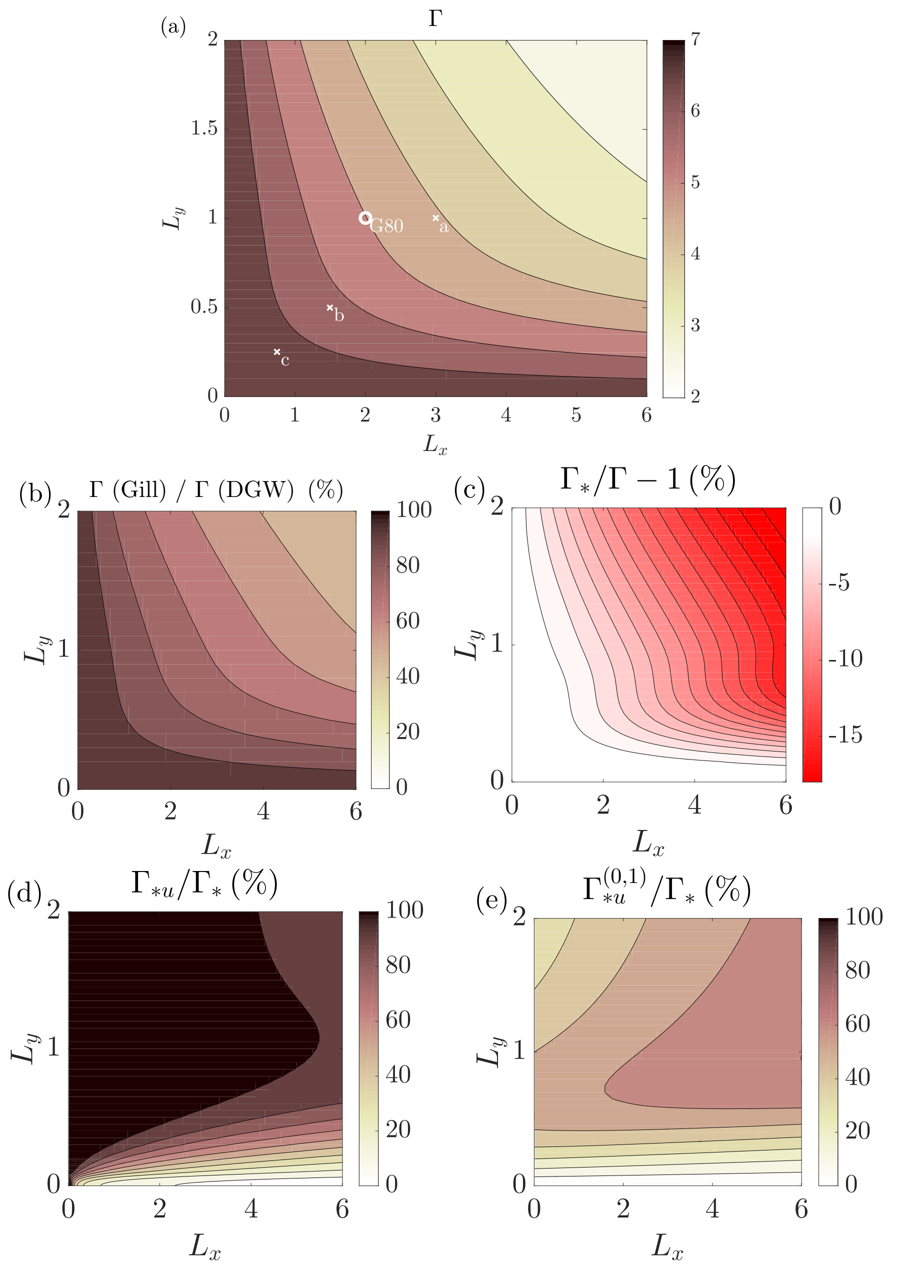


Figure 7: (a) Intensity $\Gamma$ of the overturning circulation in the rotating case; the letters "a", "b", and "c" indicate the cases shown in Figures 3 and 4 and "G80" indicates the case discussed in G80. Contours interval 0.5; (b) Ratio of the intensity of the circulation in the rotating case to that in the non-rotating case; (c) Error made by approximating $\Gamma$ by $\Gamma_*$; (d) Contribution $\Gamma_{*u}$ of the zonal flow to the overturning circulation (in % of $\Gamma_*$); and (e) Contribution $\Gamma_{*u}^{(0,1)}$ of the easterly flow to the overturning circulation (in % of $\Gamma_*$).

the non-rotating case, this approximation allows us to decompose the intensity of the overturning circulation into the sum of contributions from the different modes:

$$\Gamma_* = \sum_{n=0}^{\infty} \Gamma_*^{(2n)} = \sum_{n=0}^{\infty} \Gamma_*^{(2n,1)} + \Gamma_*^{(2n,2)}, \tag{71}$$

with $\Gamma_*^{(2n,1)}$ and $\Gamma_*^{(2n,2)}$ the contributions of the first and second part of the response to the projection of the diabatic heating $D$ on the $n^{\text{th}}$ symmetric cylinder function $D_{2n}$, i.e., $a_{2n}$ multiplied by the response to a diabatic heating in the form $F(x)D_{2n}(y)$.

$$\Gamma_*^{(2n,i)} = a_{2n} \int_{-4L_y}^{4L_y} \int_{-L_x}^{L_x} w^{(2n,i)} \, dx \, dy, \tag{72}$$

for $i = 1, 2$. Appendix B shows that we can write these contributions as:

$$\begin{aligned} \Gamma_*^{(2n,1)} &= \gamma_{2n}(L_x) f_{2n}(L_y) + [1 - \gamma_{2n}(L_x)]\, g_{2n,1}(L_y) && (73) \\ \Gamma_*^{(2n,2)} &= \gamma_{2n+2}(L_x) f_{2n}(L_y) + [1 - \gamma_{2n+2}(L_x)]\, g_{2n,2}(L_y) && (74) \end{aligned}$$

with the variation in $L_x$ given by the series of functions $\gamma_{2n}$:

$$\begin{aligned} \gamma_0 = &\quad \tfrac{1}{2} q_0^{(0)}(L_x) && = \frac{1}{2} \frac{1 + e^{-2\epsilon L_x}}{1 + \epsilon^2 l_x^2}, \\ \gamma_{2n} = &\quad \tfrac{1}{2} \tfrac{q_{2n}^{(2n)}(-L_x)}{2n-1} = \tfrac{1}{2} q_{2n}^{(2n-2)}(-L_x) && = \frac{1}{2} \frac{1 + e^{-2(4n-1)\epsilon L_x}}{1 + (4n-1)^2 \epsilon^2 l_x^2} \text{ for } n > 0, \end{aligned} \tag{75}$$

with $l_x = 1/k = 2L_x/\pi$; and the variation in $L_y$ given by:

$$\begin{aligned} f_{2n} &= a_{2n}(L_y) I_{2n} \;\text{ with }\; I_{2n} = \int_{-4L_y}^{4L_y} D_{2n} \, dy, && (76) \\ g_{2n,1} &= -\frac{8n}{4n-1} a_{2n}(L_y) D_{2n-1}(4L_y), \text{ and} && (77) \\ g_{2n,2} &= \frac{4}{4n+3} a_{2n}(L_y) D_{2n+1}(4L_y). && (78) \end{aligned}$$

Figure 8 shows these functions for $n \le 5$. In terms of amplitude, $\Gamma_*$ is dominated by the response of mode $n = 0$, because the differences $f_0 - g_{0,1} = f_0$ and $f_0 - g_{0,2}$ are the largest, and because the $\gamma_0$'s decrease with increasing $L_x$ is the slowest of all $\gamma_{2n}$. But all modes with larger $n$ also contribute to the sensitivity of $\Gamma_*$ to $L_x$ and $L_y$.

Since $\gamma_{2n}(0) = 1$, $\Gamma_*^{(2n,i)} = f_{2n}$ for all $n$ and $i = 1, 2$, and we can establish by integration that $\Gamma_*$ is an excellent approximation of $\Gamma$ in the limit $L_x \to 0$:

$$\Gamma_*(0, L_y) = 2 \int_{-4L_y}^{4L_y} \sum_{n=0}^{\infty} a_{2n} D_{2n} \, dy = 2 \int_{-4L_y}^{4L_y} D \, dy = 4\sqrt{\pi}\, \mathrm{erf}(2) = \mathrm{erf}(2)[Q]. \tag{79}$$

$\Gamma_*(0, L_y)$ is the same as in the non-rotating case and it is a good approximation of $\Gamma(0, L_y) = [Q]$. It is independent of $L_y$, which is consistent with Figure 7a. From our numerical integration, it appears that $\Gamma_*$ also tends towards a value close to $\Gamma(L_x, 0) = [Q]$ for $L_y \to 0$, as in the non-rotating case.

With $\gamma_{2n}(0) = 1$ and $\gamma_{2n} \to 0$ for $L_x \to \infty$, each contribution $\Gamma_*^{(2n,i)}$ is $f_{2n}$ for $L_x = 0$ and tends towards $g_{2n,i}$ for $L_x \to \infty$. Figure 8a shows the functions $\gamma_{2n}$ for $n$ from 0 to 5. $\gamma_0$ is identical to $\Gamma_*^{\ell=0}$ found for the non-rotating case, which is in keeping with the interpretation of the first part of the response to a diabatic heating following $D_0$ as a Kelvin wave, whose properties are the same as a gravity wave except for its latitudinal structure. The decrease of $\gamma_0$ with $L_x$ therefore results from the same processes as that of a gravity wave: the diffusive effect of large-scale circulation on temperature perturbations is less effective for smoother diabatic heating (i.e., larger $L_x$), and this results in a smaller difference between $Q$ and $\epsilon T$, and therefore a smaller vertical speed $w$ (see Eq. (32)). The decay of $\gamma_{2n}$ with $L_x$ is increasingly fast with increasing $n$, which means that the larger $n$ (and the larger $i$), the faster the convergence of the circulation response to a diabatic heating along $D_{2n}$ towards its limit $g_{2n,i}$ for $L_x \to \infty$. A more intricate latitudinal structure of the diabatic heating (i.e., a larger $n$) yields a stronger sensitivity of the circulation response to $L_x$. This differs from the non-rotating case, for which more intricate latitudinal structures of the diabatic heating (i.e., large wavenumbers $\ell$) lead to smaller sensitivity of the circulation to $L_x$. We can attribute this change in sensitivity to the effect of rotation: for larger $n$, the diabatic heating has extrema further from the equator, where the effect of rotation is larger and temperature anomalies generate circulations that are increasingly rotational and less and less convergent, creating less vertical motion.

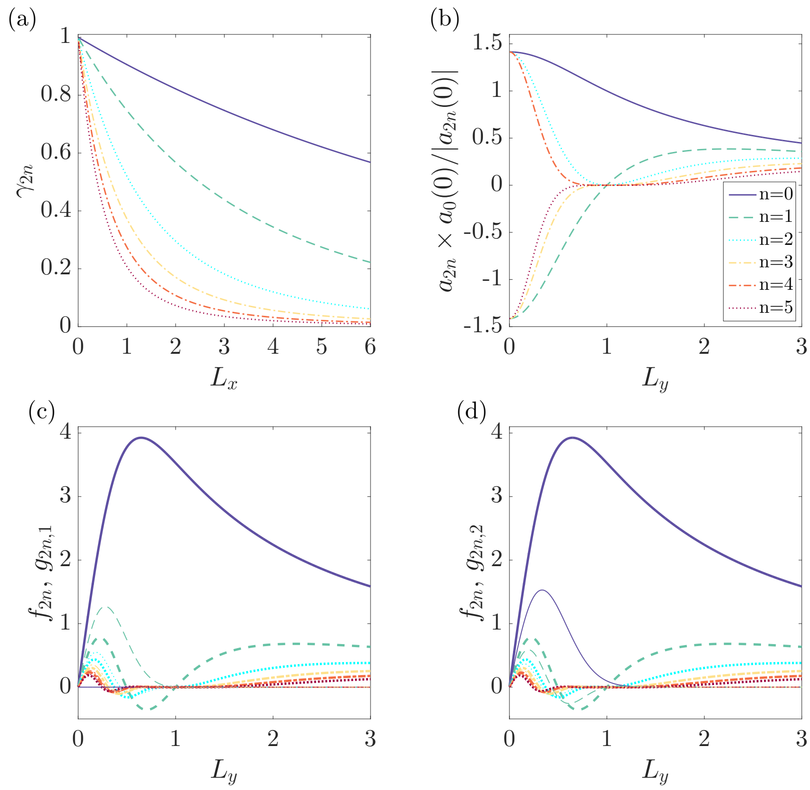


Figure 8: Functions determining the sensitivity of the contribution $\Gamma_*^{(2n,i)}$ to the longitudinal extent $L_x$ and $L_y$ of the diabatic heating for $n \leq 5$ : (a) $\gamma_{2n}(L_x)$ gives the variation of $\Gamma_*^{(2n,1)}$ and $\Gamma_*^{(2n-2,2)}$ from the $f_{2n}$ for $L_x = 0$ to, respectively, $g_{2n,1}$ and $g_{2n,2}$ for $L_x \to \infty$; (b) $a_{2n}$ the projection coefficient of $D$ on the cylinder function $D_{2n}$, normalized by $|a_{2n}(0)/a_0(0)|$; (c) $f_{2n}$ (thick lines) and $g_{2n,1}$ (thin lines) give the limits of $\Gamma_*^{(2n,1)}$ for, respectively, $L_x = 0$ and $L_x \to \infty$; and (d) $f_{2n}$ (thick lines) and $g_{2n,2}$ (thin lines) give the limits of $\Gamma_*^{(2n,2)}$ for, respectively, $L_x = 0$ and $L_x \to \infty$.

From its value for $L_x = 0$ independent from $L_y$ (see Eq. (79)), the decrease of $\Gamma_*$ with $L_x$ is determined by the limits of the circulation response to a diabatic heating along $D_{2n}$ for $L_x = 0$ (functions $f_{2n}(L_y)$) and $L_x \to \infty$ (functions $g_{2n,i}(L_y)$). These are the product of (i) the change in projection of $D$ onto the cylinder functions $D_{2n}$, given by $a_{2n}$, and (ii) the sensitivity of the dynamical response of the atmosphere to $L_y$ for diabatic heating following the cylinder function $D_{2n}$. These functions are shown in Figures 8b-d. We can distinguish two domains:

- $L_y \geq 1$: for $L_y = 1$, $D$ is $D_0$, so $a_0 = 1$ and $a_{2n} = 0$ for all $n > 0$ (and its $n-1$ first derivatives are zero as well) – this is the case described in G80. For increasing $L_y > 1$, $D$ is less and less peaked at the equator; it projects increasingly on higher and higher $n$ cylinder functions while projecting less and less on cylinder function 0, as shown in Figure 8b. Because of the exponential decay of $D_n(4L_y)$ with increasing $L_y$, $g_{2n,1}$ and $g_{2n,2}$ are negligible in this range of $L_y$ (see Fig. 8c,d), and $\Gamma_*^{(2n,i)} \approx \gamma_{2(n+i-1)}(L_x) f_{2n}(L_y)$ ($i = 1$ or 2). For the same reason, $I_{2n}$ tends towards the integral of $D_{2n}$ over $[-\infty, +\infty]$ and the variation of $f_{2n}$ with $L_y$ is determined by the variation of $a_{2n}$ (see Fig. 8b,c,d), with a decreasing contribution of mode 0 and an increasing contribution of higher and higher $n$ modes for increasing $L_y$. Considering the sensitivity of the functions $\gamma_{2n,i}(L_x)$ to $n$ explained above, the decrease of $\Gamma_*$ with $L_x$ is therefore larger for larger $L_y$. Since $\Gamma_*$ is independent of $L_y$ for $L_x$=0, this explains the sensitivity of $\Gamma_*$ to both $L_x$ and $L_y$.
- $L_y < 1$, there is still a strong influence of the response of mode $n = 0$, but the influence of modes with larger $n$ is complex. For $L_y$ close to zero, both $a_{2n}(0)$ and $I_{2n} \approx 8L_y D_{2n}(0)$ alternate sign as $(-1)^n$ (see Eqs. (36) and (A5)), so $f_{2n}$ is positive for all $n$. But $f_{2n} - g_{2n,1}$ is negative for $n > 0$ which means that the contributions to the circulation $\Gamma_*^{(2n,1)}$ increases with increasing $L_x$. $f_{2n} - g_{2n,2}$ is positive and $\Gamma_*^{(2n,2)}$ decreases with increasing $L_x$ and compensates at least partially the increase in $\Gamma_*^{(2n,1)}$. Appendix B (Eqs. (B14) and (B15)) shows that, for $L_x$ close to zero, $\Gamma_*^{(2n,2)}$ more than compensates $\Gamma_*^{(2n,1)}$: $\Gamma_*^{(2n)} = \Gamma_*^{(2n,1)} + \Gamma_*^{(2n,2)}$ decreases with $L_x$ for all $n$. This illustrates the large compensations between the two components of the response to the heating along $D_{2n}$ for each $n > 0$. For larger $L_y < 1$, $f_{2n}$, $g_{2n,1}$, $g_{2n,2}$, and their differences can change sign for $n > 0$ since $D_{2n}$ and $D_{2n\pm1}$ changes sign at least once over the interval $[-4L_y, 4L_y]$, resulting in an increase of the contributions $\Gamma_*^{(2n,i)}$ with increasing $L_x$ in intervals where $a_{2n}(f_{2n} - g_{2n,i}) < 0$. These contributions in these intervals reduce the sensitivity of $\Gamma_*$ to $L_x$ and, since $\Gamma_*(0, L_y)$ is a constant, $\Gamma_*$ is larger for reduced sensitivity to $L_x$, i.e. for smaller $L_y$. Appendix B quantifies the sensitivity of $\Gamma_*$ to $L_x$ for $L_x$ close to zero, and shows an increase of the sensitivity of $\Gamma_*$ to $L_x$ with increasing $L_y$, starting from zero sensitivity for $L_y = 0$ and increasing to large sensitivity at large $L_y$.

Despite this overall complexity, it appears clearly that the two components of the response to the heating along $D_0$ are the main contributors to $\Gamma_*$. This is because in this mode, the Kelvin-wave pattern and the Rossby-wave pattern both contribute to low level wind convergence in the region of ascent through the easterlies at the eastern boundary (for the first component) and westerlies at the western boundary (for the second component). By contrast, the two components for modes with $n > 0$ are opposite close to the equator, with gyres that circulate in opposite directions, and there is a significant amount of compensation between components of of the response to the heating along $D_{2n}$ with $n > 0$.

Thanks to the continuity equation, we can also decompose $\Gamma_*$ into the sum of a contribution from the meridional wind ($v$ integrated over the boundary at $y = \pm 4L_y$ and a contribution $\Gamma_{*u}$ from the zonal wind ($u$ integrated over the boundaries at $x = \pm L_x$). And each contribution $\Gamma_*^{(2n,i)}$ can also be decomposed in the same way, as for the non-rotating case:

$$\Gamma_* = \Gamma_{*u} + \Gamma_{*v} \quad \text{and} \quad \Gamma_*^{(2n,i)} = \Gamma_{*u}^{(2n,i)} + \Gamma_{*v}^{(2n,i)}$$

Because $u^{(0,1)}(-L_x) = 0$ and $u^{(2n,i)}(L_x) = 0$ for all $n > 0$ or $i = 2$, The contribution from the zonal wind at the eastern border results exclusively from the damped Kelvin wave extending eastward from the heating, while the contribution from the zonal wind at the western border results from a combination of damped Rossby waves. By integrating $u$ given in Equations (28)-(31), we can write:

$$\Gamma_{*u}^{(2n,1)} = \gamma_{2n}(L_x)\left[f_{2n}(L_y) - (4n-1)g_{2n,1}(L_y)\right], \tag{80}$$

$$\Gamma_{*u}^{(2n,2)} = \gamma_{2n+2}(L_x)\left[f_{2n}(L_y) + (4n+3)g_{2n,2}(L_y)\right], \tag{81}$$

and we can compute $\Gamma_{*u}$ by summing over $n$. Figure 7d shows that except for small $L_y$, $\Gamma_{*u}$ is the dominant contribution to $\Gamma_*$, unlike in the non-rotating case in which the relative contributions of $\Gamma_{*u}$ and $\Gamma_{*v}$ are similar for similar ratio $L_x/L_y$ (see Fig. 5c). The smaller contribution of the meridional wind $\Gamma_{*v}$ results from the partial compensation between the equatorward and poleward branches of the gyres. But the westerly low-level zonal flow into the ascending region through its western boundary is also part of these gyres, and it contributes very significantly to the flow. In the limit $L_x \to 0$, $\Gamma_* \approx \Gamma_{*u}$. Section 2.5 also shows that, in this limit, $w \sim Q$; this means that the region of ascent is the region of diabatic heating which extends to infinity in the latitudinal direction, so that there is no flow at the meridional boundaries. As in the non-rotating case, we have:

$$\Gamma_u \sim \Gamma \sim [Q] \text{ and } \Gamma_v \sim 0 \tag{82}$$

irrespective of $L_y$, as for the damped gravity wave (see Eq. (70)), so the contribution of the zonal flow is predominant for both $\Gamma$ and its approximation $\Gamma_*$ in this limit.

Figure 7e shows that the contribution $\Gamma_{*u}^{(0.1)}$ of the damped Kelvin wave (i.e., of the first part of the response to $D$'s projection onto $D_0$) represents a significant fraction of $\Gamma_*$ (and $\Gamma_{*u}$) except for small $L_y$. This relative contribution is larger than 60% for large $L_x$ but it can be as low as one third for small $L_x$ and large $L_y$, which shows the importance of the low-level westerly jet associated with the damped Rossby waves for small $L_x$, while for large $L_x$ the contribution of the gyres to $\Gamma_*$ results overwhelmingly from the meridional winds.

### 3.3 Equatorial westerly jet

While the damped gravity has no horizontal wind at the center of the diabatic heating, the Gill circulation is characterized by a low-level westerly jet there. This low-level jet is an interesting feature of the Gill circulation because it can increase the surface turbulent heat fluxes if the background surface wind is westerly as well (as in the Indian Ocean), or decrease them if the background wind is easterly (as over most of the rest of the equatorial belt). The resulting modulation of surface fluxes has been pointed out as a potential energy source for tropical intraseasonal variability (Sobel et al., 2008, 2010). This jet also contributes to horizontal non-linear moisture advection which is thought to contribute to the eastward propagation of tropical intraseasonal disturbances (Maloney et al., 2010; Leroux et al., 2016). The two cyclonic gyres that extend westward from the region of heating on both sides of the equator interact constructively to create this jet. On the other hand, the Kelvin-wave pattern extending eastward actually slows down this jet. As can be seen in Figure 3, as the scale of the heating decreases, the Kelvin wave signal increases slightly, but the effect of the gyres dominates: they become smaller, faster, and closer to the equator, which accelerates the low-level westerly jet but decreases its latitudinal extent.

As metrics of this jet, we will study the low-level wind speed at the center of the diabatic heating $u_o = -u(0,0)$ ($u$ describes the first baroclinic mode, so that low-level winds have the opposite sign), the zonal extent of the jet $x_u$ defined as the zonal coordinate at which $u$ changes sign along the x-axis: $u(x_u, 0) = 0$, the meridional extent of the jet $y_u$ defined as the positive meridional coordinate at which $u$ changes sign along the y-axis: $u(0, y_u) = 0$, and the integrated intensity of the jet $U = -\int_{-y_u}^{y_u} u(0,y)dy$, which describes the low-level eastward mass transport around the equator. Figure 9 shows the sensitivity of these four metrics as a function of $L_x$ and $L_y$.

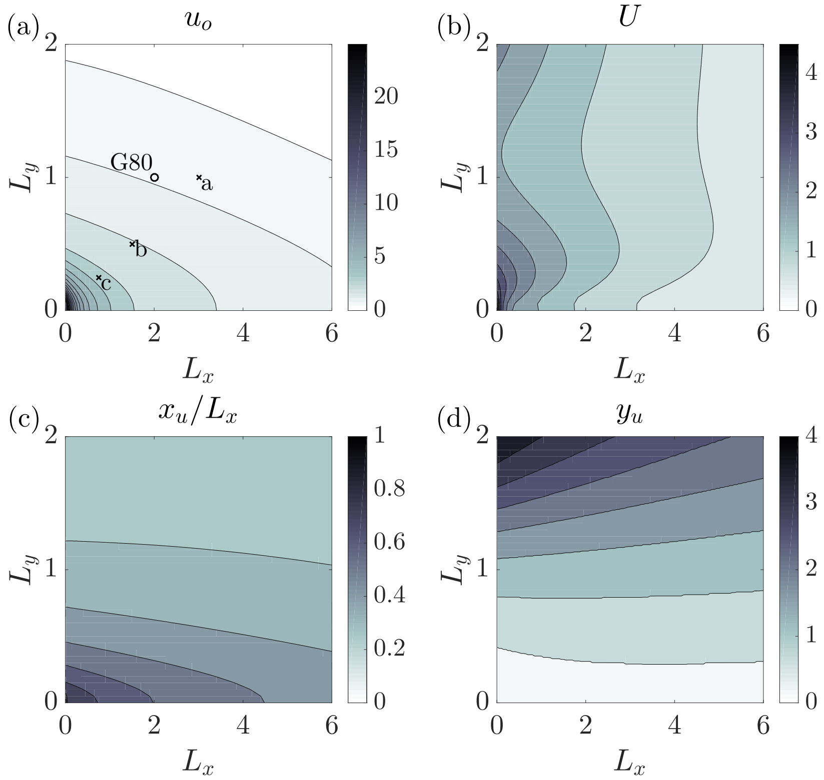


Figure 9: Characteristics of the equatorial westerly jet in the Gill circulation: (a) westerly zonal velocity at the origin $u_\text{o}$; the letters "a", "b", and "c" indicate the cases shown in Figures 3 and 4 and "G80" indicates the case discussed in G80; (b) Intensity $U$ of the jet; (c) Zonal extent $x_u$ of the jet normalized by $L_x$; (d) meridional extent $y_u$ of the jet.

The low-level equatorial wind $u_\text{o}$ at the center of the diabatic heating decreases with both $L_x$ and $L_y$ (see Fig. 9a). It tends towards zero for large $L_x$ or large $L_y$, and towards infinity if both $L_x$ and $L_y$ tend towards zero. We can also decompose $u_\text{o}$ into a sum of contributions from the different modes:

$$u_\text{o} = \sum_{n=0}^{\infty} u_\text{o}^{(2n)} = \sum_{n=0}^{\infty} u_\text{o}^{(2n,1)} + u_\text{o}^{(2n,2)}, \tag{83}$$

with $u_\text{o}^{(2n,1)}$ and $u_\text{o}^{(2n,2)}$ the contributions of the first and second components of the response to the projection of the diabatic heating $D$ on the $n^\text{th}$ symmetric cylinder function $D_{2n}$. Appendix C shows that there is a significant compensation between $u_\text{o}^{(2n,2)}$ and $u_\text{o}^{(2n,1)}$ for $n > 0$ because the two gyres straddling the equator have opposite rotation (cyclonic v.s. anticyclonic) in the two components. We can write:

$$u_\text{o}^{(2n)} = \nu_{2n}(L_x) h_{2n}(L_y), \tag{84}$$

with the variation in $L_x$ (respectively, $L_y$) encapsulated in the series of functions $\nu_{2n}$ (resp., $h_{2n}$):

$$\begin{aligned} \nu_0(L_x) &= -\frac{1}{2}q_0^{(0)}(0) + \frac{3}{2}q_2^{(0)}(0), \\ \nu_{2n}(L_x) &= -\left(n - \frac{1}{4}\right)\frac{q_{2n}^{(2n)}(0)}{2n-1} + \left(n + \frac{3}{4}\right) q_{2n+2}^{(2n)}(0), \text{ for } n > 0. \end{aligned} \quad (85)$$

$$\begin{aligned} h_0(L_y) &= a_0(L_y)D_0(0) = \sqrt{\frac{2}{1+L_y^2}}, \\ h_{2n}(L_y) &= 2a_{2n}(L_y)D_{2n}(0) = \frac{(2n)!}{(2^n n!)^2}\left(\frac{1-L_y^2}{1+L_y^2}\right)^n \sqrt{\frac{8}{1+L_y^2}}, \text{ for } n > 0. \end{aligned} \quad (86)$$

Figure 10 shows the functions $\nu_{2n}$ and $h_{2n}$ for $n \le 5$. These show that the response to the forcing along $D_0$ is the largest contribution to $u_\text{o}$ except for $L_x$ and $L_y \to 0$, but most cylinder modes do contribute to the sensitivity of $u_\text{o}$ to $L_x$ and $L_y$. The functions $\nu_{2n}$ include the two compensating effects of $u_\text{o}^{(2n,1)}$ and $u_\text{o}^{(2n,2)}$. For $h_{2n} > 0$, the contribution from $u_\text{o}^{(2n,2)}$ is positive, larger for $L_x = 0$ (scaling with $(4n+3)$), and decaying faster (with a derivative scaling with $(4n+3)^2$). The contribution from $u_\text{o}^{(2n,1)}$ is negative, smaller in amplitude (scaling with $(4n-1)$) for $L_x = 0$, and decaying slower (with a derivative scaling with $(4n-1)^2$, see Eqs. (85), (C4) and (C5)). As a result of this compensation, $\nu_{2n}(0) = 1$, independent from $n$, and $\nu_{2n}$ decreases towards 0 for $L_x \to \infty$. This decrease is faster for larger $n$, similarly to the functions $\gamma_{2n}$ which describe the sensitivity of $\Gamma_*$ to $L_x$.

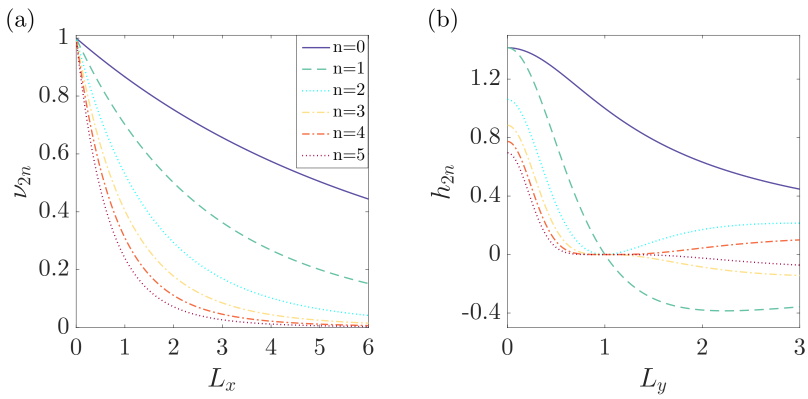


Figure 10: Functions determining the sensitivity of the contributions $u_\text{o}^{(2n)}$ to the westerly zonal velocity at the origin $u_\text{o}$ for $n \le 5$: (a) $\nu_{2n}(L_x)$ gives the variation of $u_\text{o}^{(2n)}$ with $L_x$ and (b) $h_{2n}$ gives the variation of $u_\text{o}^{(2n)}$ with $L_y$.

The functions $h_{2n}$ describe the sensitivity of $u_\text{o}^{(2n)}$ to $L_y$, which is essentially dominated by the sensitivity of $a_{2n}$ in terms of amplitude (see the similarity between Figs. 8b and 10b), but $D_{2n}(0)$ contributes to the sign: $D_{2n}(0)$'s sign is given by $(-1)^n$, while $a_{2n}$ is given by $((1-L_y^2)/(1+L_y^2))^n$; as a result, $h_{2n}$ is positive for all $n$ for $L_y < 1$ and, for $L_y > 1$, $h_{2n}$ is positive for even $n$ and negative for odd $n$. As in the case of $\Gamma_*$, we find this distinction between two regimes on each side of $L_y = 1$, for which $D = D_0$ and $a_{2n} = 0$ for $n > 0$:

- For $L_y \leq 1$, all cylinder modes interact constructively to strengthen the low-level westerly jet. The amplitudes of functions $h_{2n}$ decrease with $L_y$. For all $n > 0$, $h_{2n}(1)$ and its $(n-1)$ first derivatives are zero at $L_y = 1$; $h_{2n}$ also slowly decreases with increasing $n$ at $L_y = 0$ ($h_{2n}(0) = (1-(2n)^{-1})h_{2n-2}(0)$). $h_0$ is different, first because $h_0(1) = 1$ (case with $D = D_0$), and also because $h_0(0)$ is not larger than $h_2(0)$: this results from the specificity of the first component of the response to heating along $D_0$, i.e., the Kevin-wave pattern that extends east of the heating region and decreases the low-level westerly jet more efficiently than opposing gyres. The decrease of all $h_{2n}$ with $L_y$ in this regime results from the decrease in the amplitudes of projection coefficients $a_{2n}$ with $L_y$, which results directly from the smoother latitudinal distribution of diabatic heating. Moreover, the decrease in $|a_{2n}|$ with $L_y$ is larger for larger $n$, so that the relative contribution from cylinder modes with large $n$ decreases with $L_y$, which explains why the sensitivity to $L_x$ is maximum for $L_y = 0$ (see Fig. 9a).
- For $L_y > 1$, there is still a strong influence of the response of mode $n = 0$, and the influence of modes with larger $n$ is complex. Because $h_{2n}$ changes sign for each increment in $n$, there is considerable compensation between the contributions from successive cylinder modes. For even $n$, $h_{2n} > 0$ and $u_{\mathrm{o}}^{(2n)}$ decreases with increasing $L_x$; for odd $n$, $h_{2n} < 0$ and $u_{\mathrm{o}}^{(2n)}$ increases with increasing $L_x$ ($|u_{\mathrm{o}}^{2n}|$ decreases), which reduces the sensitivity of $u_{\mathrm{o}}$ to $L_x$. The sensitivity of $|h_{2n}|$ to $L_y$ is still controlled by that of $a_{2n}$. The projection coefficient $a_0$ decreases as $(1+L_y^2)^{-1}$, and for larger $n$ $a_{2n}$ increases from zero for $L_y = 0$ to a maximum for a value of $L_y$ that increases with $n$, and decreases for larger $L_y$, because $D$ projects more and more on modes that have significant amplitude further and further away from the equator (i.e., on $D_{2n}$ of increasing $n$) as $L_y$ increases. As a result, the contribution to the low-level westerly jet from cylinder modes with $n > 0$ comes largely from a subset of modes with similar $n$, with a lot of compensation between modes, and as a result, the sensitivity to $L_y$ results mostly from the sensitivity of the projection of $D$ on the cylinder mode $n = 0$. For $L_y \to \infty$, the contribution of cylinder modes with larger and larger $a_{2n}$ gets relatively larger, but all projections coefficients $a_{2n}$ tend rapidly to zero, so that the sum $u_{\mathrm{o}}$ also tends to zero.

Figure 9c shows the eastward longitudinal extent $x_u$ of the low-level westerly jet normalized by $L_x$. For small $L_x$ and $L_y$, $x_u \sim L_x$, which means that the westerly jet extends over the whole region of diabatic heating at the equator, $x_u$ decreases with $L_y$, and increases significantly slower than $L_x$ when $L_x$ is increased. For very large $L_x$ or $L_y$, $x_u$ tends towards zero (not shown), which means that the zonal flow becomes more symmetrical in longitude with respect to the center of heating, with westerlies to the west and easterlies to the east, more similar to the damped gravity wave. Figure 9d shows, on the other hand, that the latitudinal extent $y_u$ of the low-level westerly jet increases with both $L_x$ and $L_y$. For $L_y \to 0$, $y_u$ is small but non-zero except if $L_x \to 0$ as well, in which case $y_u$ scales like $2L_y$. This scaling is approximately valid for larger values of $L_y$ and $L_x \to 0$, showing that the region of westerlies scales with the region of heating. For $L_x > 0$, this widening is less pronounced, but $y_u$ still increases faster than $L_y$ for the interval of $L_x$ considered here. As a result, while $y_u$ increases slightly with increasing $L_x$ for $L_y \to 0$, it decreases with $L_x$ for $L_y > 0.7$. The sensitivities of $y_u$ and $u_{\mathrm{o}}$ help explain that of the intensity $U$ of the low-level westerly jet shown in Figure 9b: as the velocity $u_{\mathrm{o}}$ at the center of the jet decreases with $L_y$, its latitudinal extent $y_u$ increases, and as a result, $U$ is not very sensitive to $L_y$. On the other hand, $U$ decreases with $L_x$ because of the dominant influence of $u_{\mathrm{o}}$. Using Equation (62) in Section 2.5, we can write find the following scalings for the limit $L_x, L_y \to 0$:

$$\begin{aligned} u_{\mathrm{o}} &\sim \frac{2}{L_y}, &(87)\\ x_u &\sim L_x, &(88)\\ y_u &\sim 2L_y, \text{ and} &(89)\\ U &\sim 2\sqrt{\pi}\,\mathrm{erf}(1) + 4e^{-1}. &(90)\end{aligned}$$

Note that the maximum westerly wind is at the equator, west of the center of heating. For $L_x \to 0$, it is the furthest from the heating center, at $(-L_x, 0)$; in this limit, the maximum scales like $2u_o$.

## 4 Summary and conclusion

In this article, we explore the scale sensitivity of the equatorial Gill circulation, focusing on characteristics of this circulation likely to couple it with the energy cycle: we study the sensitivity of the intensity overturning circulation (total mass upward/downward flux), which interacts with moist processes, and the characteristics of the low-level westerly flow in the region where the diabatic heating is imposed, which influences turbulent surface heat fluxes. In all our experiments, we impose the same horizontally-integrated diabatic heating in order to understand how the dynamical response of the atmosphere depends on how spatially concentrated the diabatic heating is. This makes sense in terms of energy cycle: if we consider that the overall evaporation is at first order constant, the amount of latent heat available to be released in the atmosphere is fixed, and analogous reasoning can apply to other atmospheric energy sources. In this Part I, we study the case of diabatic heating symmetric about the equator (Part II studies asymmetric cases). We also compare our results with the non-rotating case, which is a damped gravity wave.

We find that the intensity of the overturning circulation decreases with both the longitudinal and the latitudinal extents of the diabatic heating, and more than for the damped gravity wave. For the damped gravity wave, the weakening of the damped-gravity-wave circulation with increasing scales can be explained by the equivalence of vertical energy transport with a diffusive process on temperature; as a result, the temperature perturbation $T$ is relatively smoother than the diabatic heating $Q$. This diffusive effect is more efficient at small scales than at large scales, and the pattern difference between $T$ and $Q$ is therefore larger at small scales than at large scales. This results in a larger $w = Q - \epsilon T$ at small scales than at large scales. In the Gill circulation, this sensitivity is enhanced by the influence of rotation which transforms the divergent circulation of the damped gravity wave into a Kelvin-wave structure east of the diabatic heating and cyclonic gyres straddling the equator west of the heating center. While the Kelvin-wave component exhibits some similarity with a gravity wave with meridional wavenumber zero, the cyclonic gyres have a very different structure and sensitivity. As a result, the decrease in intensity of the overturning circulation with the horizontal scales is about three times faster than in the non-rotating case.

As for the low-level westerly jet in the region diabatic heating, we find that for most metrics, it is relatively smaller and weaker for large horizontal scales than for small ones. The velocity at the center of the jet decreases with increasing scales, the latitudinal and longitudinal extents of the jet increase with increasing scales, but slower than the latitudinal and longitudinal scales of the diabatic heating. For very small scales, the jet extends eastward all the way to the eastern boundary of the diabatic heating. The total zonal mass flux in this jet decreases with the longitudinal extent of the diabatic heating, but its sensitivity to the latitudinal extent is small.

Our results suggest that the coupling of the Gill circulation with the hydrologic cycle would result in a stronger moisture convergence for small heating regions than for large heating regions. Since we can reasonably assume that the imposed diabatic heating results from latent and radiative heating in a convective cloud cluster, this means that the moisture-convergence feedback would be stronger for small clusters than for large ones if the circulation is in quasi-equilibrium with the diabatic heating. Furthermore, our results also show that the low-level westerly jet is stronger and overlaps with a larger region of diabatic heating for small scales than for large scales. This suggest that the coupling with surface turbulent fluxes would result in a decrease of surface fluxes in easterlies and an increase in turbulent fluxes in westerlies via the wind-induced surface heat exchange mechanism. Over most of the tropics where trade winds are dominant, this would cause a negative feedback to a diabatic heating perturbation. Over the Indian Ocean where the dominant surface winds flow eastward, this would become a positive feedback.

Although our results are significant in general for the steady or slowly evolving tropical circulations, they are particularly significant in the case of the MJO. More than four decades after the discovery of this phenomenon, the fundamental mechanisms of the MJO are still debated (Majda et al., 2007; Chen & Stechmann, 2015; Sobel & Maloney, 2012, 2013; Yano & Tribbia, 2017; Rostami & Zeitlin, 2019), and a better understanding of the circulation associated with this convective disturbance contributes to this debate. While the dynamical signature of the MJO resembles the symmetric solution described in G80, its latitudinal scale is smaller, and the scale sensitivity of the overturning circulation combined with its coupling to the hydrologic cycle might contribute to explaining the MJO scale selection. Also, the MJO convective disturbances do grow in the equatorial westerlies of the Indian Ocean, and some studies have suggested that these background winds are crucial to their development (Sobel et al., 2008, 2010; Maloney et al., 2010; Leroux et al., 2016), particularly because of wind-induced surface-heat-flux feedback described above, but also because of horizontal moisture advection; the scale sensitivity of the low-level westerly jet suggests that such mechanisms are particularly active in small clusters, i.e. during the development of MJO disturbances.

## Appendix A A few properties of the cylinder functions $D_n$

The cylinder functions $D_n$ are defined by the recursive Equation (12). They also verify, as pointed out by G80 (their Equations (3.7) and (3.8)):

$$\frac{dD_n}{dy} + \frac{y}{2} D_n = n D_{n-1}, \tag{A1}$$

$$\frac{dD_n}{dy} - \frac{y}{2} D_n = -D_{n+1}, \tag{A2}$$

and they are solutions of the differential equations:

$$\frac{d^2 D_n}{dy^2} + \left(n + \frac{1}{2} - \frac{y^2}{4}\right) D_n = 0. \tag{A3}$$

$D_{2n}$ are even functions and $D_{2n+1}$ are odd functions of $y$. We have:

$$D_{2n+1}(0) = 0 = \frac{dD_{2n}}{dy}(0), \tag{A4}$$

$$D_{2n}(0) = -(2n+1) D_{2n-2}(0) = \left(-\tfrac{1}{2}\right)^n \tfrac{(2n)!}{n!} = -\frac{dD_{2n+1}}{dy}(0). \tag{A5}$$

Using Equations (A1) and (A2), we can also write:

$$\int_{Y_1}^{Y_2} D_{n+1}\, dy = n \int_{Y_1}^{Y_2} D_{n-1}\, dy - 2\left[D_n(Y_2) - D_n(Y_1)\right]. \tag{A6}$$

## Appendix B Contributions of the cylinder modes to $\Gamma_*$

By using the expressions of $w^{(2n,i)}$ ($i = 1$ or 2) in Equation (32) combined with the expressions of $T^{(2n,i)}$ from Equations (30) and (31) we can write $\Gamma_*^{(2n,i)}$ as:

$$\Gamma_*^{(2n,1)} = \frac{a_{2n}}{2}\left(\int_{-L_x}^{L_x} F\, dx\ I_{2n} - \epsilon \int_{-L_x}^{L_x} q_{2n}^{(2n)}\, dx\ \left[I_{2n} + 2n I_{2n-2)}\right]\right), \tag{B1}$$

$$\Gamma_*^{(2n,2)} = \frac{a_{2n}}{2}\left(\int_{-L_x}^{L_x} F\, dx\ I_{2n} - \epsilon \int_{-L_x}^{L_x} q_{2n+2}^{(2n)}\, dx\ \left[I_{2n+2} + (2n+2) I_{2n)}\right]\right), \tag{B2}$$

for all $n$. We have introduced the notation $I_{2n} = \int_{-4L_y}^{4L_y} D_{2n}\, dy$ for $n \geq 0$ and $I_{-2} = 0$.

The integral of $F$ is:

$$\int_{-L_x}^{L_x} F\, dx = 2,$$

and the differential Equations (18) and (21) yield the following expressions for the integrals of the functions $q_{2n(+2)}^{(2n)}$:

$$\epsilon \int_{-L_x}^{L_x} q_0^{(0)}\, dx = 2 - q_0^{(0)}(L_x), \tag{B3}$$

$$\epsilon \int_{-L_x}^{L_x} q_{2n}^{(2n)}\, dx = \frac{1}{4n-1}\left[4n - 2 - q_{2n}^{(2n)}(-L_x)\right] \quad \text{for } n > 0, \tag{B4}$$

$$\text{and } \epsilon \int_{-L_x}^{L_x} q_{2n+2}^{(2n)}\, dx = \frac{1}{4n+3}\left[2 - q_{2n+2}^{(2n)}(-L_x)\right] \quad \text{for all } n, \tag{B5}$$

in which we have used $q_0^{(0)}(-L_x) = 0$, $q_{2n}^{(2n)}(L_x) = 0$ for $n > 0$, and $q_{2n+2}^{(2n)}(L_x) = 0$ for all $n$.

Equation (A6) yields:

$$I_{2n-2} = \frac{1}{2n-1}\left(I_{2n} + 4D_{2n-1}(4L_y)\right) \quad \text{and} \quad I_{2n+2} = (2n+1)I_{2n} - 4D_{2n+1}(4L_y). \tag{B6}$$

Using Equations (B3)-(B6), Equations (B1) and (B2) can be rewritten:

$$\Gamma_*^{(0,1)} = \frac{q_0^{(0)}(L_x)}{2} a_0 I_0, \tag{B7}$$

$$\Gamma_*^{(2n,1)} = \frac{q_{2n}^{(2n)}(-L_x)}{4n-2} a_{2n} I_{2n} - \frac{8n}{4n-1} a_{2n} D_{2n-1}(4L_y)\left(1 - \frac{q_{2n}^{(2n)}(-L_x)}{4n-2})\right) \quad \text{for } n > 0, \tag{B8}$$

$$\Gamma_*^{(2n,2)} = \frac{q_{2n+2}^{(2n)}(-L_x)}{2} a_{2n} I_{2n} + \frac{4}{4n+3} a_{2n} D_{2n+1}(4L_y)\left(1 - \frac{q_{2n+2}^{(2n)}(-L_x)}{2})\right) \quad \text{for all } n. \tag{B9}$$

By replacing $q_{2n}^{(2n)}$ by its expression from Equations (24) and (26), and using $q_{2n}^{(2n)} = (2n-1)q_{2n}^{(2n-2)}$, $\Gamma_*^{(2n,i)}$ can be written as in Equations (73) and (74).

Using the differential Equations (18) and (21), the partial derivative of these contributions with respect to $L_x$ for $L_x = 0$ can be written:

$$\frac{\partial \Gamma_*^{(0,1)}}{\partial L_x}(0, L_y) = -\epsilon f_0(L_y), \tag{B10}$$

$$\frac{\partial \Gamma_*^{(2n,1)}}{\partial L_x}(0, L_y) = -(4n-1)\epsilon\left(f_{2n}(L_y) - g_{2n,1}(L_y)\right) \quad \text{for } n > 0, \tag{B11}$$

$$\frac{\partial \Gamma_*^{(2n,2)}}{\partial L_x}(0, L_y) = -(4n+3)\epsilon\left(f_{2n}(L_y) - g_{2n,2}(L_y)\right) \quad \text{for all } n. \tag{B12}$$

Using the iterative Equations (A1)-(A3), each $\Gamma_*^{(2n,i)}$ can be rewritten as a function of $D_{2n}$ only:

$$\frac{\partial \Gamma_*^{(0,1)}}{\partial L_x}(0, L_y) = -2\epsilon a_0 I_0 - \epsilon a_0\left[-2I_0 + 8L_y D_0(4L_y) + \int_{-4L_y}^{+4L_y} \frac{y^2}{2} D_0 dy\right], \tag{B13}$$

$$\frac{\partial \Gamma_*^{(2n,1)}}{\partial L_x}(0, L_y) = -\epsilon a_{2n}\left[-2I_{2n} + 8L_y D_{2n}(4L_y) + \int_{-4L_y}^{+4L_y} \frac{y^2}{2} D_{2n} dy\right] \quad \text{for } n > 0, \tag{B14}$$

$$\frac{\partial \Gamma_*^{(2n,2)}}{\partial L_x}(0, L_y) = -\epsilon a_{2n}\left[2I_{2n} - 8L_y D_{2n}(4L_y) + \int_{-4L_y}^{+4L_y} \frac{y^2}{2} D_{2n} dy\right] \quad \text{for all } n. \tag{B15}$$

Although far from the simplest forms, these equations show that there is a lot of compensation between the sensitivity of $\Gamma_*^{(2n,1)}$ to $L_x$ for small $L_x$ and $\Gamma_*^{(2n,2)}$ for $n > 0$, and also they yield a simple expression for $\Gamma_*^{(2n)}$:

$$\frac{\partial \Gamma_*^{(0)}}{\partial L_x}(0, L_y) = -\epsilon a_0\left[2I_0 + \int_{-4L_y}^{+4L_y} y^2 D_0 dy\right] \quad \text{and} \tag{B16}$$

$$\frac{\partial \Gamma_*^{(2n)}}{\partial L_x}(0, L_y) = -\epsilon a_{2n} \int_{-4L_y}^{+4L_y} y^2 D_{2n} dy \quad \text{for } n > 0, \tag{B17}$$

which shows that, for $L_x$ close to 0, each circulation $\Gamma_*^{(2n)}$ in response to the diabatic heating projection onto $D_{2n}$ decreases with $L_x$. Summing over $n$, we get the following sensitivity of $\Gamma_*$ to $L_x$:

$$\frac{\partial \Gamma_*}{\partial L_x}(0, L_y) = -2\epsilon a_0 I_0 - \epsilon \int_{-4L_y}^{+4L_y} y^2 D dy. \tag{B18}$$

Integrating by parts and using changes in variables yields:

$$\frac{\partial \Gamma_*}{\partial L_x}(0, L_y) = -4\epsilon \left[ \sqrt{\frac{2\pi}{1+L_y^2}} \operatorname{erf}(2L_y) + \left(\sqrt{\pi}\operatorname{erf}(2) - 4e^{-4}\right) L_y^2 \right]. \tag{B19}$$

Both terms inside the brackets are zero for $L_y = 0$ and positive otherwise, which shows that the change of $\Gamma_*$ with $L_x$ for small $L_x$ is zero for $L_y$ =0, and increasingly negative for increasing $L_y$. The first term results from mode $n = 0$, and varies almost linearly with $L_y$ for small $L_y$, but tends to zero for $L_y \to \infty$, while the second terms results from all other modes and increases quadratically in $L_y$.

The contribution $\Gamma_{*u}^{(2n,i)}$ to $\Gamma_*^{(2n,i)}$ from the zonal flow is simply the integral of the zonal velocity $u^{(2n,i)}$ over the zonal boundary of the the rectangle $(2L_x, 8L_y)$ where it is not zero, multiplied by $\pm a_{2n}$. Using Equations (28), (30), and (31), it can be written as:

$$\Gamma_{*u}^{(0,1)} = \frac{a_0}{2} q_0^{(0)}(L_x) I_0 = \Gamma_*^{(0,1)}, \tag{B20}$$

$$\Gamma_{*u}^{(2n,1)} = -\frac{a_{2n}}{2} q_{2n}^{(2n)}(-L_x)\left[I_{2n} - 2nI_{2n-2}\right] \quad \text{for } n > 0, \tag{B21}$$

$$\Gamma_{*u}^{(2n,2)} = -\frac{a_{2n}}{2} q_{2n+2}^{(2n)}(-L_x)\left[I_{2n+2} - (2n+2)I_{2n}\right] \quad \text{for all } n. \tag{B22}$$

The last two can be simplified using Equation (B6) into:

$$\Gamma_{*u}^{(2n,1)} = \frac{q_{2n}^{(2n)}(-L_x)}{4n-2} a_{2n}\left[I_{2n} + 8nD_{2n-1}(4L_y)\right] \quad \text{for } n > 0, \tag{B23}$$

$$\Gamma_{*u}^{(2n,2)} = \frac{q_{2n+2}^{(2n)}(-L_x)}{2} a_{2n}\left[I_{2n} + 4D_{2n+1}(4L_y)\right] \quad \text{for all } n. \tag{B24}$$

By replacing $q_{2n}^{(2n)}$ by its expression from Equations (24) and (26), and using $q_{2n}^{(2n)} = (2n-1)q_{2n}^{(2n-2)}$, $\Gamma_{*u}^{(2n,i)}$ can be written as in Equations (80) and (81).

## Appendix C Contributions of the cylinder modes to $u_{\mathrm{o}}$

By using the expressions of $u^{(2n,i)}$ ($i = 1$ or 2) in Equations (30) and (31) we can write $u_{\mathrm{o}}^{(2n,i)}$ as:

$$u_{\mathrm{o}}^{(0,1)} = -\frac{a_0}{2} q_0^{(0)}(0) D_0(0), \tag{C1}$$

$$u_{\mathrm{o}}^{(2n,1)} = -\frac{a_{2n}}{2} q_{2n}^{(2n)}(0)\left[D_{2n}(0) - 2nD_{2n-2}(0)\right] \text{ for } n > 0, \tag{C2}$$

$$u_{\mathrm{o}}^{(2n,2)} = -\frac{a_{2n}}{2} q_{2n+2}^{(2n)}(0)\left[D_{2n+2}(0) - (2n+2)D_{2n}(0)\right] \text{ for all } n \tag{C3}$$

Using Equation (A5), we can express the linear combinations of cylinder functions at $y = 0$ as proportional to $D_{2n}(0)$:

$$u_{\mathrm{o}}^{(2n,1)} = -\frac{a_{2n}}{2} q_{2n}^{(2n)}(0) \frac{4n-1}{2n-1} D_{2n}(0), \tag{C4}$$

$$u_{\mathrm{o}}^{(2n,2)} = \frac{a_{2n}}{2} q_{2n+2}^{(2n)}(0)(4n+3) D_{2n}(0), \tag{C5}$$

for all $n$. $u^{(0,1)}$ is the westward wind associated with the Kevin-wave response. $u_{\mathrm{o}}^{(2n,1)}$ is the westward equatorial branch of the anticyclonic gyres along the equator for $n >$

0 and $u_\mathrm{o}^{(2n,2)}$ is the eastward equatorial branch of the cyclonic gyres along the equator. They both scale with $n$, but there is considerable compensation between $u_\mathrm{o}^{(2n,1)}$ and $u_\mathrm{o}^{(2n,2)}$, and therefore it does not provide any insight to present them independently. Their sum yield Equation (84).

**Acknowledgments**

The authors thank Jean-Philippe Duvel for his useful comments. The authors also acknowledge the support of the University of Auckland, and particularly financial support from its Faculty of Science in the form a PhD fellowship and a grant from the Faculty Research Development Fund. G.B. is also supported by the Glavish-Buckley Lectureship.

## References

Abramowitz, M., & Stegun, I. A. (1964). *Handbook of Mathematical Functions with Formulas, Graphs, and Mathematical Tables* (ninth Dove ed.). New York: Dover.

Adam, O. (2018). Zonally Varying ITCZs in a Matsuno-Gill-Type Model With an Idealized Bjerknes Feedback. *Journal of Advances in Modeling Earth Systems*, *10*(6), 1304–1318. doi: 10.1029/2017MS001183

Battisti, D. S., Sarachik, E. S., & Hirst, A. C. (1999). A Consistent Model for the Large-Scale Steady Surface Atmospheric Circulation in the Tropics*. *Journal of Climate*, *12*(10), 2956–2964. doi: 10.1175/1520-0442(1999)012⟨2956:ACMFTL⟩2.0.CO;2

Bellon, G. (2011). Monsoon intraseasonal oscillation and land–atmosphere interaction in an idealized model. *Climate Dynamics*, *37*(5-6), 1081–1096. doi: 10.1007/s00382-010-0893-0

Bellon, G., & Reboredo, B. (2020). Scale sensitivity of the gill circulation, Part II: off-equatorial case. *Journal of Advances in Modeling Earth Systems*, submitted.

Bellon, G., & Sobel, A. (2010). Multiple equilibria of the hadley circulation in an intermediate-complexity axisymmetric model. *Journal of Climate*, *23*, 1760–1778.

Bellon, G., & Sobel, A. H. (2008). Poleward-Propagating Intraseasonal Monsoon Disturbances in an Intermediate-Complexity Axisymmetric Model. *Journal of the Atmospheric Sciences*, *65*(2), 470–489. doi: 10.1175/2007JAS2339.1

Bretherton, C. S., & Sobel, A. H. (2003). The Gill Model and the Weak Temperature Gradient Approximation. *Journal of the Atmospheric Sciences*, *60*(2), 451–460. doi: 10.1175/1520-0469(2003)060⟨0451:TGMATW⟩2.0.CO;2

Cane, M. A., & Zebiak, S. E. (1985). A Theory for El Nino and the Southern Oscillation. *Science*, *228*(4703), 1085–1087. doi: 10.1126/science.228.4703.1085

Cauchy, A. L. B. (1821). *Cours d'analyse de l'École Royale Polytechnique: Analyse algébrique. I.re partie.* Paris: Debure frères.

Chen, S., & Stechmann, S. N. (2015). Nonlinear traveling waves for the skeleton of the Madden-Julian oscillation. *ArXiv e-prints*.

Gill, A. E. (1980). Some simple solutions for heat-induced tropical circulation. *Quarterly Journal of the Royal Meteorological Society*, *106*(449), 447–462. doi: 10.1002/qj.49710644905

Heckley, W. A., & Gill, A. E. (1984). Some simple analytical solutions to the problem of forced equatorial long waves. *Quarterly Journal of the Royal Meteorological Society*, *110*(463), 203–217. doi: 10.1002/qj.49711046314

Hendon, H. H., & Salby, M. L. (1994). The Life Cycle of the Madden–Julian Oscillation. *Journal of the Atmospheric Sciences*, *51*(15), 2225–2237. doi: 10.1175/1520-0469(1994)051⟨2225:TLCOTM⟩2.0.CO;2

Kiladis, G. N., Straub, K. H., & Haertel, P. T. (2005). Zonal and Vertical Structure of the Madden–Julian Oscillation. *Journal of the Atmospheric Sciences*, *62*(8), 2790–2809. doi: 10.1175/JAS3520.1

Krueger, A. F., & Winston, J. S. (1974). A Comparison of the Flow Over the Tropics During Two Contrasting Circulation Regimes. *Journal of the Atmospheric Sciences*, *31*(2), 358–370. doi: 10.1175/1520-0469(1974)031⟨0358:ACOTFO⟩2.0.CO;2

Leroux, S., Bellon, G., Roehrig, R., Caian, M., Klingaman, N. P., Lafore, J.-P., … Tyteca, S. (2016). Inter-model comparison of subseasonal tropical variability in aquaplanet experiments: Effect of a warm pool. *Journal of Advances in Modeling Earth Systems*, *8*(4), 1526–1551. doi: 10.1002/2016MS000683

Lin, J.-L., Mapes, B. E., & Han, W. (2008). What Are the Sources of Mechanical Damping in Matsuno–Gill-Type Models? *Journal of Climate*, *21*(2), 165–179. doi: 10.1175/2007JCLI1546.1

Lin, J.-L., Zhang, M., & Mapes, B. (2005). Zonal Momentum Budget of the Madden–Julian Oscillation: The Source and Strength of Equivalent Linear Damping. *Journal of the Atmospheric Sciences*, *62*(7), 2172–2188. doi: 10.1175/jas3471.1

Lintner, B. R., Bellon, G., Sobel, A. H., Kim, D., & Neelin, J. D. (2012). Implementation of the Quasi-equilibrium Tropical Circulation Model 2 (QTCM2): Global simulations and convection sensitivity to free tropospheric moisture. *Journal of Advances in Modeling Earth Systems*, *4*, M12002. doi: 10.1029/2012MS000174

Madden, R. A., & Julian, P. R. (1971). Detection of a 40–50 Day Oscillation in the Zonal Wind in the Tropical Pacific. *Journal of the Atmospheric Sciences*, *28*(5), 702–708. doi: 10.1175/1520-0469(1971)028⟨0702:DOADOI⟩2.0.CO;2

Majda, A. J., Stechmann, S. N., & Khouider, B. (2007). Madden Julian Oscillation analog and intraseasonal variability in a multicloud model above the equator. *Proceedings of the National Academy of Sciences*, *104*(24), 9919–9924. doi: 10.1073/pnas.0703572104

Maloney, E. D., Sobel, A. H., & Hannah, W. M. (2010). Intraseasonal variability in an aquaplanet general circulation model. *Journal of Advances in Modeling Earth Systems*, *2*, 5. doi: 10.3894/JAMES.2010.2.5

Neelin, J. D., & Zeng, N. (2000). A Quasi-Equilibrium Tropical Circulation Model—Formulation*. *Journal of the Atmospheric Sciences*, *57*(11), 1741–1766. doi: 10.1175/1520-0469(2000)057⟨1741:AQETCM⟩2.0.CO;2

Pazan, S. E., & Meyers, G. (1982). Interannual Fluctuations of the Tropical Pacific Wind Field and the Southern Oscillation. *Monthly Weather Review*, *110*(6), 587–600. doi: 10.1175/1520-0493(1982)110⟨0587:IFOTTP⟩2.0.CO;2

Philander, S. G. H. (1983). El Niño Southern Oscillation phenomena. *Nature*, *302*(5906), 295–301. doi: 10.1038/302295a0

Rostami, M., & Zeitlin, V. (2019). Eastward-moving convection-enhanced modons in shallow water in the equatorial tangent plane. *Physics of Fluids*, *31*(2), 021701. doi: 10.1063/1.5080415

Sobel, A. H., & Maloney, E. (2012). An Idealized Semi-Empirical Framework for Modeling the Madden–Julian Oscillation. *Journal of the Atmospheric Sciences*, *69*(5), 1691–1705. doi: 10.1175/JAS-D-11-0118.1

Sobel, A. H., & Maloney, E. (2013). Moisture Modes and the Eastward Propagation of the MJO. *Journal of the Atmospheric Sciences*, *70*(1), 187–192. doi: 10.1175/JAS-D-12-0189.1

Sobel, A. H., Maloney, E. D., Bellon, G., & Frierson, D. M. (2008). The role of surface heat fluxes in tropical intraseasonal oscillations. *Nature Geoscience*, *1*(10), 653–657. doi: 10.1038/ngeo312

Sobel, A. H., Maloney, E. D., Bellon, G., & Frierson, D. M. (2010). Surface fluxes and tropical intraseasonal variability: A reassessment. *Journal of Advances in Modeling Earth Systems*, *2*, 1–27. doi: 10.3894/JAMES.2010.2.2

Sobel, A. H., & Neelin, J. D. (2006). The boundary layer contribution to intertropical convergence zones in the quasi-equilibrium tropical circulation model framework. *Theoretical and Computational Fluid Dynamics*, *20*(5-6), 323–350. doi: 10.1007/s00162-006-0033-y

Yano, J.-I., & Tribbia, J. J. (2017). Tropical Atmospheric Madden–Julian Oscillation: A Strongly Nonlinear Free Solitary Rossby Wave? *Journal of the Atmospheric Sciences*, *74*(10), 3473–3489. doi: 10.1175/jas-d-16-0319.1

Zeng, N., Neelin, J. D., & Chou, C. (2000). A Quasi-Equilibrium Tropical Circulation Model—Implementation and Simulation*. *Journal of the Atmospheric Sciences*, *57*(11), 1767–1796. doi: 10.1175/1520-0469(2000)057⟨1767:AQETCM⟩2.0.CO;2

Zhang, C. (2005). Madden-Julian Oscillation. *Reviews of Geophysics*, *43*(2), RG2003. doi: 10.1029/2004RG000158

Zhang, Z., & Krishnamurti, T. N. (1996). A Generalization of Gill's Heat-Induced Tropical Circulation. *Journal of the Atmospheric Sciences*, *53*(7), 1045–1052. doi: 10.1175/1520-0469(1996)053⟨1045:AGOGHI⟩2.0.CO;2